Acta Neuropathologica (2024) 148:2
https://doi.org/10.1007/s00401-024-02763-5

ORIGINAL PAPER

Cleavage site-directed antibodies reveal the prion protein in humans is shed by ADAM10 at Y226 and associates with misfolded protein deposits in neurodegenerative diseases

Feizhi Song[1] · Valerija Kovac[2] · Behnam Mohammadi[1] · Jessica L. Littau[1] · Franka Scharfenberg[3] · Andreu Matamoros Angles[1] · Ilaria Vanni[4] · Mohsin Shafiq[1] · Leonor Orge[5,6] · Giovanna Galliciotti[1] · Salma Djakkani[1] · Luise Linsenmeier[1] · Maja Černilec[2] · Katrina Hartman[2] · Sebastian Jung[7] · Jörg Tatzelt[7,8] · Julia E. Neumann[1,9] · Markus Damme[3] · Sarah K. Tschirner[10,11] · Stefan F. Lichtenthaler[10,11,12] · Franz L. Ricklefs[13] · Thomas Sauvigny[13] · Matthias Schmitz[14] · Inga Zerr[14] · Berta Puig[15] · Eva Tolosa[16] · Isidro Ferrer[17] · Tim Magnus[15] · Marjan S. Rupnik[18] · Diego Sepulveda-Falla[1] · Jakob Matschke[1] · Lojze M. Šmid[19] · Mara Bresjanac[19] · Olivier Andreoletti[20] · Susanne Krasemann[1] · Simote T. Foliaki[21] · Romolo Nonno[4] · Christoph Becker-Pauly[3] · Cecile Monzo[22] · Carole Crozet[22] · Cathryn L. Haigh[21] · Markus Glatzel[1] · Vladka Curin Serbec[2] · Hermann C. Altmeppen[1]

Received: 24 April 2024 / Revised: 28 June 2024 / Accepted: 3 July 2024

Abstract

Proteolytic cell surface release ('shedding') of the prion protein (PrP), a broadly expressed GPI-anchored glycoprotein, by the metalloprotease ADAM10 impacts on neurodegenerative and other diseases in animal and in vitro models. Recent studies employing the latter also suggest shed PrP (sPrP) to be a ligand in intercellular communication and critically involved in PrP-associated physiological tasks. Although expectedly an evolutionary conserved event, and while soluble forms of PrP are present in human tissues and body fluids, for the human body neither proteolytic PrP shedding and its cleavage site nor involvement of ADAM10 or the biological relevance of this process have been demonstrated thus far. In this study, cleavage site prediction and generation (plus detailed characterization) of sPrP-specific antibodies enabled us to identify PrP cleaved at tyrosin 226 as the physiological and apparently strictly ADAM10-dependent shed form in humans. Using cell lines, neural stem cells and brain organoids, we show that shedding of human PrP can be stimulated by PrP-binding ligands without targeting the protease, which may open novel therapeutic perspectives. Site-specific antibodies directed against human sPrP also detect the shed form in brains of cattle, sheep and deer, hence in all most relevant species naturally affected by fatal and transmissible prion diseases. In human and animal prion diseases, but also in patients with Alzheimer`s disease, sPrP relocalizes from a physiological diffuse tissue pattern to intimately associate with extracellular aggregated deposits of misfolded proteins characteristic for the respective pathological condition. Findings and research tools presented here will accelerate novel insight into the roles of PrP shedding (as a process) and sPrP (as a released factor) in neurodegeneration and beyond.

Keywords Alzheimer's disease · Dementia · Extracellular vesicles · Neuroprotection · Prions · Proteolytic processing

Abbreviations

aa	Amino acid
Ab	Antibody
Aβ	Amyloid-beta peptide
AD	Alzheimer's disease
ADAM	A disintegrin and metalloproteinase
AIDS	Acquired immunodeficiency syndrome
APP	Amyloid precursor protein
BSA	Bovine serum albumin
BSE	Bovine spongiform encephalopathy
CAA	Cerebral amyloid angiopathy
CJD	Creutzfeldt–Jakob disease
cKO	Conditional knockout
CNS	Central nervous system
CSF	Cerebrospinal fluid
CWD	Chronic wasting disease
DMSO	Dimethyl sulfoxide

Feizhi Song, Valerija Kovac, Behnam Mohammadi and Hermann C. Altmeppen are equally contributing authors.

Extended author information available on the last page of the article

Published online: 09 July 2024

EV	Extracellular vesicles
FBS	Fetal bovine serum
FFPE	Formalin-fixed paraffin-embedded
fl-PrP	Full length prion protein
GI	GI254023X (ADAM10 inhibitor)
GPI	Glycosylphosphatidylinositol
GW	GW280264X (ADAM inhibitor)
HIV	Human immunodeficiency virus
IF	Immunofluorescence
iPSC	Induced pluripotent stem cells
KO	Knockout
NaDOC	Sodium deoxycholate
ND	Neurodegeneration
PBS	Phosphate-buffered saline
PI	Protease inhibitor
PI-PLC	Phosphatidylinositol-specific phospholipase C
PMA	Phorbol 12-myristate 13-acetate
Prnp$^{0/0}$	PrP^{C} knockout
PrP^{C}	Cellular prion protein
PrP^{Sc}	Pathological (Scrapie) isoform of the prion protein
(Q-)PICS	(Quantitative) proteomics for the identification of cleavage sites
RIPA	Radioimmunoprecipitation assay (buffer)
sPrP	Shed PrP
$sPrP^{G227}$	Antibody against murine shed PrP
$sPrP^{Y226}$	Antibody against human shed PrP
TACE	Tumor necrosis factor α converting enzyme (ADAM17)
TAILS	Terminal amine isotopic labeling of substrates
TBS	Tris-buffered saline
TCA	Trichloroacetic acid
TMA	Tissue microarray
TPS	Total protein stain
V5B2	Monoclonal antibody-directed against human shed PrP (PrP^{Y226})
WB	Western blot
WT	Wild type
Y226	Tyrosine at position 226 (PrP sequence)

Introduction

Proteolytic processing is of utmost importance for regulating certain proteins' physiological functions, yet also plays important roles in diverse pathological conditions [67]. For some "multifunctional" proteins, conserved cleavages by endogenous proteases do not just simply reflect a start of inactivation or catabolic degradation, but rather represent the impetus for functional diversity, regulation and effects mediated by the resulting fragments. The prion protein (PrP), a membrane-anchored glycoprotein with high (though not exclusive) expression in the nervous system, may be considered as a multifunctional protein, at least in view of the variety of suggested physiological tasks [2, 9, 69, 70]. In contrast, its key pathological role in fatal and transmissible neurodegenerative prion diseases such as Creutzfeldt–Jakob disease (CJD), where it serves as the critical substrate for a templated and progressive misfolding and aggregation process resulting in neuronal death and brain vacuolization, is firmly established [3, 21, 103, 123]. And a relevant role of PrP as a neuronal cell surface receptor for other toxic protein conformers in more common neurodegenerative diseases (such as Alzheimer's (AD) or Parkinson's disease) is being increasingly recognized [22, 25, 30, 36, 64, 96, 105].

Some conserved endogenous cleavage events within PrP have been identified over the years, yet their biological relevance is just starting to be understood as more systematic studies are being conducted [19, 40, 66, 70, 130]. This also applies to the constitutive, membrane-proximate shedding by the metalloprotease ADAM10 [5, 14, 122], which is of particular interest as it releases nearly full-length PrP, i.e., shed PrP (sPrP), into the extracellular space while leaving only the GPI-anchor and a few amino acids behind at the plasma membrane. This cleavage not only is a critical mechanistic part of a compensatory network ensuring cellular PrP homeostasis [72]. It also impacts on neurodegenerative diseases by reducing cell surface PrP as a relevant receptor for (neuro) toxic protein assemblies [47, 93]. Moreover, once released into the extracellular space and interstitial fluid, sPrP may block, detoxify and sequester harmful oligomers into less toxic deposits [71, 93], as observed earlier for recombinant PrP (recPrP) in vitro or transgenically expressed PrP dimers serving as a proxy for physiologically shed PrP [12, 18, 33, 88, 95, 113]. Fittingly, in prion disease mouse models, ADAM10 expression correlates with incubation and survival time [4, 28]; and sPrP levels inversely correlate with PrP^{Sc} formation [4, 32, 42, 71, 93]. This collectively supports the notion that soluble PrP forms like sPrP may indeed act as "prion replication antagonists" [44, 53, 88, 136]. Recent studies in transgenic mice also highlight an influence of the ADAM10-mediated PrP shedding on prion strain characteristics and resulting aggregate morphology [1, 116]. Hence, manipulation of this particular proteolytic process appears to be a promising option against neurodegenerative diseases [47, 71, 93]. We have recently uncovered a substrate-specific approach to this in murine cells and tissue using PrP-directed ligands [71], thereby avoiding general targeting of ADAM10 and, hence, likely side effects by affecting its manifold substrates in different organs [108, 134].

Apart from neurodegenerative conditions, recent studies on potential biological roles of sPrP suggest it to act as a ligand inducing effects in different recipient cell types, regulating cellular differentiation, homeostasis, morphogenesis and immunological processes [7, 78–81]. Depending on the pathophysiological context, sPrP may also play detrimental

roles as suggested by studies linking it with elevated inflammatory responses in HIV neuropathogenesis [86] as well as trophic effects or drug-resistance in cancer [101, 135]. In sum, these studies indicate sPrP as a novel factor in intercellular communication with likely cell-, tissue- and context-dependent consequences, and highlight the need for further investigations on protective as well as potentially harmful functions of sPrP in the nervous system and beyond. However, as those studies mainly used recPrP as a non-physiological proxy for bona fide sPrP, this may pose limitations regarding interpretation of the findings, as—for instance—differences in structure or glycosylation state may very well influence biological effects and experimental outcome [93].

Though providing critical initial insight, most studies on biological roles played by sPrP were limited to in vitro or animal models, thus leaving an important gap of knowledge for the human system. Moreover, when it comes to systematically investigating effects of PrP shedding and intrinsic functions of sPrP in meaningful models, there is at least one major hurdle: in brain or other tissue samples, and even in body fluids, reliable detection of sPrP using pan-PrP antibodies is difficult given the vastly exceeding and masking amounts of full-length membrane-bound PrP [either cell-associated or on extracellular vesicles (EVs)] with almost similar molecular weight and a current lack of discriminating antibodies [93, 130]. For the murine system, we have recently overcome this problem by generating cleavage site-specific antibodies for sPrP (not detecting its uncleaved GPI-anchored precursor [72]) based on the previously published cleavage site [122]. For the human body, however, strictly speaking neither the proteolytic C-terminal shedding in general, nor clear (and potentially sole) involvement of ADAM10 in this process or the respective cleavage site within PrP have been convincingly shown or identified to date. This is surprising given that constitutive and reactive PrP release by different human cell types with likely (patho) physiological relevance, and presence of respective soluble, nearly full-length PrP forms in human brain tissue, cerebrospinal fluid (CSF) and blood have been shown manifold over the last 3 decades [39, 48, 61, 76, 98, 99, 120]. Moreover, reports on the existence of nearly full-length, C-terminally truncated PrP variants in some prion disease patients, caused by stop mutations [46] or as yet unknown reasons [23, 27, 75, 117, 132], were followed by speculations on a potential link between such fragments and proteolytic shedding [57].

Supported by structural cleavage site predictions, we generated, characterized and compared poly- and monoclonal antibodies specifically detecting physiological C-terminally shed PrP in human samples. By demonstrating both the cleavage site at position Y226↓Q227 and functionality of these antibodies in different paradigms, we also show a clear and apparently exclusive ADAM10 dependency of respective signals. Further, as previously demonstrated in murine samples [71], we show that shedding can be stimulated by PrP-directed antibodies in different models of human origin and discuss its therapeutic feasibility. We assess PrP shedding in central nervous system (CNS) tissue, CSF and various cell types using different technical approaches. Using heterologous expression models, we also show that murine ADAM10 is able to cleave human PrP at the 'human' cleavage site, while human ADAM10 on murine PrP employs G227↓R228, the proper cleavage site in mice and rats. Strikingly, because of similar C-terminal sequences, the antibodies for human sPrP presented herein also detect shed PrP fragments in some of the most prion disease-relevant animal species such as cattle, sheep/goats, and deer, thus likely enabling future studies on the relevance of PrP shedding in bovine spongiform encephalopathy (BSE), Scrapie and chronic wasting disease (CWD), respectively. Lastly, we address PrP shedding in samples of patients affected by neurodegenerative diseases including CJD and AD, and demonstrate that sPrP, in the presence of proteopathic aggregates, is redistributed from an originally nondescript and diffuse to a plaque-associated pattern, thus warranting further studies on the proposed role of sPrP in blocking and sequestering extracellular toxic oligomers into potentially less harmful deposits. Moreover, we suggest future investigations to assess sPrP's potential as an (easily) accessible biomarker in body fluids. In conclusion, we here provide novel information and research tools to study a formerly underestimated yet increasingly appreciated and evolutionary conserved proteolytic cleavage event on a key player in neurodegenerative proteinopathies, with therapeutic potential and biological relevance probably not being restricted to the CNS.

Materials and methods

Samples and ethics statements

Human samples

Postmortem human tissues (FFPE blocks and frozen samples) were acquired in the framework of diagnostic hospital and reference center activities. Use of such tissue samples (following data protection-conform anonymization) after conclusion of diagnostic procedures was in agreement with §12 of the Hamburg Hospital Act (*Hamburgisches Krankenhausgesetz*; HmbKHG) and regulations at the University Medical Center Hamburg-Eppendorf, and follows ethical regulations of the 1964 Declaration of Helsinki, its later amendments or comparable ethical standards; CSF samples: approved by the institutional review board of the independent ethics committee of the Hamburg Chamber of Physicians (PV3392).

Tissue samples (Fig. 6b–e) were obtained for diagnostic purposes from mandatory autopsies under surveillance rules and in agreement with local ethic guidelines. They were provided upon anonymization by Prof. Dr. Mara Popović (Institute of Pathology, Faculty of Medicine, University of Ljubljana, Slovenia), Prof. Dr. Herbert Budka (Division of Neuropathology and Neurochemistry, Medical University Vienna, Austria) and Prof. Dr. James Ironside, Neuropathology Laboratory, National CJD Surveillance Unit, University of Edinburgh, Edinburgh, UK.

Frozen brain samples (Fig. 7a) were obtained from the Institute of Neuropathology Brain Bank (now a branch of the HUB-ICO-IDIBELL Biobank) Hospitalet de Llobregat, Barcelona, Spain. This procurement was carried out in compliance with Spanish biomedical research regulations, including *Ley de la Investigación Biomédica* 2013 and *Real Decreto de Biobancos* 2014, and approval of the Ethics Committee of the Bellvitge University Hospital (HUB) PI-2019/108.

Information on human samples analysed in this study is summarized in Table 1.

Human embryonic NSCs were purchased from Thermo Fisher Scientific, approval number NOR/REC R0500096A (French Biomedicine Agency). The human iPSC cells used for organoids were purchased from ATCC and de-identified before being provided to the researchers at the NIH. Their use has been reviewed and determined to be exempt from IRB review; Approval number: 17-NIAID-00212, 3rd of August 2017.

Animal samples

No experiments on living animals were performed for this study, as in accordance with the '3R' principles in animal research, we profited from samples already available from previous studies. Breeding and sacrification for the sake of organ removal were approved by the ethical research committees of respective national/local authorities: *Freie und Hansestadt Hamburg–Behörde für Gesundheit und Verbraucherschutz*, Hamburg, Germany (ORG1023 for WT (C57BL/6J) and PrP-KO ($Prnp^{0/0}$) mice); *Schleswig-Holsteinisches Ministerium für Energiewende, Landwirtschaft, Umwelt und ländliche Räume*, Kiel, Germany (V241-25481/2018(30-3/16) for the 5xFAD mouse). Frozen brains (used for western blot (WB) analyses) of transgenic mouse lines tg338 (sheep-VRQ), tg501 (goat-ARQ), tg110 (bovine), tg340 (human-MM129), and tg361 (human-VV129) were obtained from the breeding colony of *Istituto Superiore di Sanità*, Rome, Italy. These lines are on a $Prnp^{0/0}$ background and homozygous for the transgene. Approved and supervised by the Service for Biotechnology and Animal Welfare of the *Istituto Superiore di Sanità* and authorized by the Italian Ministry of Health (decree number: 1119/2015-PR). All procedures were carried out in accordance with the Italian Legislative *Decree* 26/2014 and European Union (EU) Council directives 86/609/EEC and 2010/63/EU. Samples of prion-infected transgenic mice (Fig. 6 and Supplementary Fig. 10): Procedures were in compliance with institutional and French national guidelines and with aforementioned EU directives. Experiments were approved by the Committee on the Ethics of Animal Experiments of INRAe Toulouse/ENVT (Permit Number: 01734.01).

Brains of BSE-infected cattle and a Scrapie-infected sheep (Fig. 6c) were archived veterinarian samples of naturally occurring prion diseases.

Frozen animal brain samples (Supplementary Fig. 7) were obtained from postmortem examination in the framework of diagnostic activities of the National Institute for Agricultural and Veterinary Research (INIAV), Portugal. Use of these samples upon finished diagnostic procedures was reviewed and approved by the Quality and Environment Office of the INIAV. Samples were non-biohazardous and non-infectious.

Cell lines

All mammalian cell lines used in this study are listed in Table 2. For human NSCs and iPSCs see text above.

Cell culture treatments and harvesting of lysates and conditioned media

Cells were treated with 30 µM of metalloprotease inhibitors GI254023X (GI) and/or GW280264X, 50 nM of the ADAM10 stimulators PMA or Carbachol, or PrP-directed antibodies (as indicated) in OptiMEM for 18 h at 37 °C with 5% CO_2. Samples were then harvested for further analysis by WB. Conditioned media was collected into cooled tubes on ice (already containing 20 × pre-dissolved protease inhibitor cocktail (PI; cOmplete EDTA-free, Roche) and subsequently centrifuged at 500×*g* and 5000×*g* for 5 min at 4 °C. The remaining supernatant was used for precipitation (as described below). The confluent cells were washed with cold PBS before addition of 150 µL of RIPA buffer (50 mM Tris–HCl pH 8, 150 mM NaCl, 1% NP-40, 0.5% Na-Deoxycholate, 0.1% SDS) containing freshly added 1 × PI for 15 min on ice. Cells were scrapped, transferred to a tube and stored on ice (with short vortexing every 5 min) for 15 min. Centrifugation was performed at 12,000×*g* for 10 min at 4 °C and supernatants (lysates) stored in aliquots at − 80 °C or mixed with water and 4 × sample buffer (SB; 250 mM Tris–HCl, 8% SDS, 40% glycerol, 20% β-mercaptoethanol (β-ME), 0.008% bromophenol blue (pH 6.8)), denatured at 96 °C for 10 min and used for SDS-PAGE. Deglycosylation of samples using PNGase F enzyme was performed according to manufacturer`s instructions (New England Biolabs).

Table 1 Details on human samples used in this study

ID	Sex	Age (y)	Diagnosis/staging/other	PMI	Method	Fig	Braak stage
1	♀	85	Control, non-ND, Cx, Cb	n.a	IHC	6	n.a
2	♂	67	sCJD (MM2C type)	n.a	IHC	6, S9	n.a
3	♂	60	sCJD (MV2K type)	n.a	IHC	6, S9	n.a
4	♀	70	sCJD (VV2 type)	n.a	IHC	S9	n.a
5	♀	64	sCJD (with Kuru plaques)	n.a	IHC, IF	6	n.a
6	♂	62	vCJD	n.a	IHC, IF	6	n.a
7	♀	41	GSS (P102L mutation)	n.a	IF	6	n.a
TMA 1	♂	67	Control, non-ND	n.a	IHC	7	–
TMA 2	♂	69	AD (CERAD C), mild CAA	n.a	IHC	7	IV
TMA 3	♂	69	Control, non-ND, brain metastasis	n.a	IHC	7	–
TMA 4	♀	98	AD (CERAD C)	n.a	IHC	7	V
AD1	♀	64	Trisomy 21 (CERAD C), front. Cx	n.a	IF	7	V
AD2	♀	76	AD (CERAD C), CAA, disease onset at 69 y, occip. Cx	8 h	BVI, IF, IHC	7, S12	VI
AD3	♀	61	AD (CERAD C), CAA, disease onset at 55 y, occip. Cx	4 h	BVI, IF, IHC	7, S12	VI
Control A1	♂	61	Non-ND, stroke	4 h	WB	7	–
Control A2	♂	78	Non-ND, stroke	2 h	WB	7	–
Control A3	♀	75	Non-ND, stroke	3 h	WB	7	–
Control A4	♂	67	Non-ND, stroke	5 h	WB	7	–
Control A5	♂	85	Non-ND, stroke	6 h	WB	7	–
Control A6	♂	64	Non-ND, mesial sclerosis	3 h	WB	7	–
Control A7	♂	71	Non-ND, no neuropathol. findings	12 h	WB	7	–
Control A8	♂	52	Non-ND, no neuropathol. findings	5 h	WB	7	–
AD B1	♂	63	AD	4 h	WB	7	I
AD B2	♀	74	AD (CERAD A)	3 h	WB	7	I
AD B3	♀	57	AD (CERAD A)	5 h	WB	7	I
AD B4	♀	75	AD	5 h	WB	7	II
AD B5	♂	66	AD	21 h	WB	7	II
AD B6	♀	72	AD	8 h	WB	7	II
AD B7	♀	77	AD	3 h	WB	7	II
AD B8	♂	65	AD	15 h	WB	7	II
AD B9	♂	57	AD	4 h	WB	7	II
AD D1	♀	83	AD	4 h	WB	7	V
AD D2	♂	79	AD	5 h	WB	7	V
AD D3	♂	75	AD	11 h	WB	7	V
AD D4	♀	85	AD (CERAD C)	16 h	WB	7	V
AD D5	♂	77	AD (CERAD C)	8 h	WB	7	V
AD D6	♀	72	AD (CERAD C)	9 h	WB	7	V
CSF_1	♀	78	Non-ND, normal pressure hydrocephalus	Biopsy	WB	7	–
CSF_2	♀	46	Non-ND, cerebral gliosis, migraine	Biopsy	WB	7	–

AD Alzheimer's disease, *BVI* brain vessel isolation, *CAA* cerebral amyloid angiopathy, *Cx* cortex, *ND* neurodegeneration, *IF* immunofluorescence analysis, *PMI* postmortem interval, *WB* SDS-PAGE and western blot analysis, *S* supplementary figure

In experiments requiring depletion of EVs from conditioned media, treatments (with antibodies, PMA and/or GI) were for 48 h. Ultracentrifugation was performed at 4 °C and 140,000×*g* for 70 min in an OPTIMA Max XP (TLA 110 rotor, Beckman Coulter). Supernatants were further precipitated (see below) and the (EV) pellet dissolved in a mixture of RIPA/sample buffer (1×).

Transfection of cells for transient overexpression (e.g., of PrP versions) were done using Lipofectamine 2000 (Thermo Fisher Scientific) according to manufacturer`s instructions. The construct for GFP-tagged PrP fusion protein (PrP-GFP) was previously cloned from pDrive-PrP^C-EGFP into the expression vector pIRES (MCS B)

Table 2 List of cell lines used in this study

Name	Origin (species, tissue)	Source	Procedures
N2a WT	Murine, neuroblastoma	Institute of Neuropathology, UKE, Hamburg (based on ATCC [CCL-131] ordered via DSMZ [ACC 148])	–
N2a PrP KO	Murine, neuroblastoma	Dr. Michael William, LMU, Munich [92]	Transfected with WT human PrP, and GFP-tagged versions of both species' PrPs (Fig. 5b)
SH-SY5Y	Human, neuroblastoma (differentiated from a metastatic bone tumor)	Institute of Neuropathology, UKE, Hamburg (based on ATCC [CRL-2266])	Transfected with human and murine PrP (Fig. 5c)
A549	Human, lung carcinoma	WT, ADAM10 KO[a] and ADAM17 KO: S. Lichtenthaler, Munich [49] WT, ADAM10 KO[b]: generated/customized for the Institute of Neuropathology, UKE, Hamburg, by the company *Ubigene*	Treatment with protease inhibitors and/or PMA
SHEP2 (Tet2)	Human, neuroblastoma	Institute of Biochemistry, University of Kiel, Germany; origin: NKI/AMC Amsterdam, The Netherlands (accession # CVCL_HF70; www.cellosaurus.org);	Treatment with antibodies or protease inhibitor
LN235	Human, astrocytoma	Prof. Dr. M. E. Hegi, Neurosurgery & Neuroscience Research Center, Epalinges; Centre hospitalier universitaire Vaudois, Lausanne Switzerland (accession # CVCL_3957; www.cellosaurus.org)	Treatment with antibodies or protease inhibitor
U373-MG	Human, glioblastoma	Merck/Sigma-Aldrich, #8061901 (accession # CVCL_2818; www.cellosaurus.org)	Treatment with antibodies or protease inhibitor

using *Sal1-XbaI* restriction sites, with the GFP tag being located between amino acids 222/223 (murine sequence).

Structural modeling (peptide-protein docking) and cleavage site prediction

The 3D conformation of the human PrP peptide 217-YERESQAYYQRGS-230 was initially predicted using PEP-FOLD3 [125]. To generate a starting template for subsequent flexible docking using the Rosetta FlexPepDock protocol [74], the peptide was aligned onto the crystal structure of the ADAM10 catalytic domain in complex with the C-terminal region of an adjacent ADAM10 molecule as substrate (PDB: 6BE6). Structure visualization and analysis were carried out using PyMOL (Schrödinger LLC). IceLogo plots for cleavage preferences of ADAM10 and ADAM17 were published earlier as indicated.

Generation of sPrP-directed antibodies

The polyclonal sPrP^{Y226} antibody was generated (upon structural prediction of Y226 as a potential shedding site) using an anti-peptide approach following a standard 87-day polyclonal protocol (Eurogentec, Belgium). Briefly, based on the sequence information of human PrP^{C}, a recombinant peptide (*N-term*-C-ESQAY**Y**-COOH; with Y-COOH representing Y226, i.e. the assumed new C-terminus of shed PrP exposed upon shedding) was produced and N-terminally coupled to *Megathura crenulata* keyhole limpet hemocyanin (KLH) as carrier protein. This immunogen was injected into two rabbits at days 0, 14, 28 and 56 of the immunization programme. Blood samples were collected from the tails at days 0, 38 and 66 for monitoring the success of the immunization process by standardized ELISA tests. Animals were killed and blood collected at day 87. Standardized quality measures at Eurogentec revealed good target responses for both final bleeds and additional affinity purification was then performed on one of the sera: a second peptide (*N-term*-C-YERESQAY**Y**QRGS; representing the C-terminus of fl-PrP till the GPI-anchor attachment site) was produced, coupled to a resin and served as a "negative control" to eliminate all antibodies from the polyclonal serum that would otherwise bind to fl-PrP.

Mouse monoclonal antibody V5B2 was generated several years ago against peptide P1 (PrP214–226, CITQYERESQAYY) in BALB/c mice [23, 132]. Three groups of five BALB/c mice were injected subcutaneously on day 0 with 0.2 mg of peptide P1 bound to KLH (P1–KLH) in Freund's complete adjuvant (0.2 mL/mouse). On days 14 and 28, the mice were injected intraperitoneally with 0.1 mg P1–KLH in Freund's incomplete adjuvant (IFA; 0.2 mL/mouse). Blood was taken from the tail vein 10 days after

the last inoculation. Antibodies against KLH, P1–KLH and peptide alone were detected in sera by indirect ELISA. A final booster dose of P1–KLH was injected on day 45 intravenously in physiological saline (0.1 mg/mouse in 0.1 mL) to mice with the highest titers of mAbs against each of the peptides. Mice were killed on day 48 and their spleens removed. Splenocytes were isolated and fused with mouse NS1 myeloma cells using 50% PEG for 3 min, according to standard techniques. Cells were washed and resuspended in 96-well microtiter plates in DMEM (Dulbecco's modification of Eagle's medium, ICN Biomedical) supplemented with 13% bovine serum (Hy Clone) (subsequently designated DMEMbov) and with feeder cells of mouse thymocytes. The next day, DMEMbov supplemented with hypoxanthine–aminopterin–thymidine (HAT, Sigma) mixture was added to all wells. Presence of specific antibodies was determined in the supernatants after 10–14 days by indirect ELISA. Hybridomas from positive wells were transferred into larger volumes of HAT-DMEMbov and the specificity of antibodies was determined by immunohistochemistry and dot blot. Selected hybridomas were cloned in DMEMbov by the limiting dilution method and frozen in liquid nitrogen. Monoclonal antibodies were purified from the cell culture supernatants by affinity chromatography on Protein G Sepharose (Sigma), using 0.1 M glycine, pH 2.7, for elution. The clone V5B2, back then, was shown to target human PrP ending at Y226 [54] and to detect certain disease-associated PrP forms in different prion diseases [23, 27, 75, 117]. The identity of the V5B2 target PrP226* as physiological shed PrP was revealed during the course of the study presented here.

Antibodies

Apart from the abovementioned antibodies for the specific detection of sPrP, all other primary antibodies employed in this study (incl. application/source) are listed in Table 3.

Recombinant prion protein production

Full-length human PrP (recPrP23-231) and truncated versions thereof (recPrP23-226, recPrP90-224, recPrP90-225, recPrP90-226, recPrP90-227, recPrP90-228, recPrP90-231) were prepared at the *Slovenian Institute for Transfusion Medicine* and expressed, purified and refolded according to our previous protocol [58]. Plasmids encoding the variant sequences were transformed into competent *E. coli* BL21 (DE3) and grown at 37 °C in 1 L of minimal medium with ampicillin (100 µg/mL), 4 g/L glucose and 1 g/L ammonium chlorid. At an OD600 of 0.8, the expression was induced with isopropyl-β-D-galactopyranoside to a final concentration of 0.8 mM. Cells were harvested 12 h after induction and lysed by sonication (Q55 Sonicator, Qsonica). Inclusion bodies were washed in buffer containing 25 mM Tris–HCl, 5 mM EDTA and 0.8% Triton X-100 (pH 8) and then in bi-distilled water several times. The isolated inclusion bodies were solubilized in 6 M GndHCl and purified on a 5 mL FF Crude HisTrap column (GE Healthcare), equilibrated in binding buffer [2 M GndHCl, 500 mM NaCl, 20 mM Tris–HCl and 20 mM imidazole (pH 8)]. Proteins were eluted with 500 mM imidazole and dialysed against 6 M GndHCl using Amicon centrifugal filters (MW cut-off: 3000 Da, Millipore). Purified proteins were stored at − 80 °C or refolded by dialysis against refolding buffer [20 mM sodium acetate and 0.005% NaN_3 (pH 4.5)] using Snake-Skin™ Dialysis Tubing (MW cut-off: 3500 Da, Thermo Scientific). Purified proteins were analyzed by SDS-PAGE under reducing conditions.

ELISA

Microtiter plates (CORNING 9018, Costar) were coated with either 50 µL of recombinant human PrP C-terminally ending at Y226 (recPrP23-226; 0.5 µg/mL) or peptide 'P1' (5 µg/mL) in ELISA coating buffer (carbonate/bicarbonate buffer, pH 9.6), incubated overnight at 4 °C, washed with PBS/Tween20 (buffer B) and then blocked with 1% bovine serum albumin in PBS/Tween20 (buffer C) (Sigma–Aldrich). 50 µL of mouse monoclonal V5B2 or rabbit polyclonal $sPrP^{Y226}$, titrated in buffer C, were added to the wells and incubated for 90 min at 37 °C. Plates were washed in buffer B, and 50 µL of HRP-conjugated anti-mouse or anti-rabbit immunoglobulin (Jackson ImmunoResearch), both diluted 1:2000 in buffer C, were added and incubated for 90 min at 37 °C. After final washes, 2,2′-azino-bis (3-ethylbenzthiazoline-6-sulfonic acid) (ABTS, Sigma-Aldrich) substrate was added to each well. Absorbance was measured at 405 nm after 10 min of incubation at 37 °C in a Tecan Sunrise microplate spectrometer (Tecan).

Human neural stem cells culture, neuronal differentiation, and treatment

We used HuPrP-overexpressing H9NSC cells (derived from human embryonic stem cells (WAO9, Wicells)). These cells were obtained following transduction of H9NSC with the pWPXL-PrP-IRES-GFP lentivirus coding for wild-type human PrP as well as GFP. These lentiviral vectors were derived from the HIV-based Tronolab vectors and produced by the Biocampus PVM Vectorology Platform. For the treatment of neurons derived from HuPrPH9NSC, amplified HuPrPH9NSC were seeded at a density of 9.6×10^5 cells per well on 6-well plates coated with Geltrex in StemProNSC medium and placed in a 37 °C, 5% CO_2 and 5% O_2 incubator. Three replicas for the four experimental groups were prepared. The day after seeding, the medium was replaced

Table 3 List of antibodies used in this study

Name/target	Description	Application	Company/source
$sPrP^{G227}$	Rb polycl. specific for mouse/rat sPrP	WB, IHC, IF	UKE Hamburg
POM1	Ms monocl. anti-PrP (C-term. half)	T, WB	Millipore
POM2	Ms monocl. anti-PrP (N-term. half)	T, WB	Millipore
3F4	Ms monocl. anti-human PrP (central)	T, WB, IHC, IF	Millipore
6D11	Ms monocl. anti-PrP (central)	T, WB	BioLegend
SAF84	Ms monocl. anti-PrP/anti-PrP^{Sc}	IHC	Cayman Chemicals
SAF70	Ms monocl. anti-PrP/anti-PrP^{Sc}	IF	Cayman Chemicals
EP1802Y	Rb monocl. anti-PrP (C-term. epitope)	WB	Abcam
β-actin	Ms monocl. anti-β-actin, clone C4	WB	Millipore
β-Tubulin III	Ms monocl. anti-β-tubulin III, clone Tuj1	IF	Covance
CD81	Rb monocl anti-CD81, clone D3N2D	WB	Cell signaling
GAPDH	Rb monocl. anti-GAPDH	WB	Cell signaling
BAM-10	Ms monocl. anti-human β amyloid	IF, IHC	Medac-Diagnostika
6E10	Ms monocl. anti-human β amyloid	WB, IHC, IF	BioLegend
APP/sAPPα	Rb polycl. anti-mouse/rat β amyloid	WB	BioLegend
ADAM10	Rb monocl. anti-ADAM10 [EPR5622]	WB	Abcam
ADAM17	Rb monocl. anti-ADAM17	WB	Abcam
Laminin	Rb polycl. anti-human Laminin	IF	Sigma-Aldrich
Lectin GS-II	Alexa 488 conj. anti-human Lectin	IF	ThermoFischer Scientific
Iba1	Rb polycl. anti-Iba1	IHC	Wako Chemicals
GFAP	Ms monocl. anti-GFAP	IHC	DAKO
LAMP1	Rat monocl. anti-Ms LAMP1 clone 1D4B	IF	Developmental Studies Hybridoma Bank (DSHB)
NF-L	Ms monocl. anti-NF-L	IF	Invitrogen
OSP	Rb polycl. anti-OSP	IF	Abcam
FoxG1	Rb polycl. anti-FoxG1	IF	Abcam
s100b	Rb monocl. anti-s100β	IF	Abcam
GABA B R1	Ms monocl. anti GABA B R1	IF	Abcam
–	Gt anti-Ms secondary/HRP	WB	Promega
–	Gt anti-Rb secondary/HRP	WB	Promega
IRDye 800 CW	Dk anti-Ms IgG	WB	Licor
IRDye 680 RD	Dk anti-Rb IgG	WB	Licor
–	Gt anti-Ms secondary/AlexaFluor-488	IF	ThermoFischer Scientific
–	Gt anti-Rb secondary/AlexaFluor-647	IF	ThermoFischer Scientific
–	Dk anti-Rb secondary/AlexaFluor-488	IF	ThermoFischer Scientific
–	Dk anti-Rb secondary/AlexaFluor-555	IF	ThermoFischer Scientific
–	Dk anti-Ms secondary/AlexaFluor-647	IF	ThermoFischer Scientific
–	Ch anti-Rb secondary/AlexaFluor-647	IF	ThermoFischer Scientific

WB western blot, *IHC* immunohistochemistry, *IF* immunofluorescence microscopy, *T* treatment, *HRP* horse radish peroxidase, *Ms* mouse, *Rb* rabbit, *Gt* goat, *Dk* donkey, *Ch* chicken, *conj* conjugated

by a N2 + bFGF 20 ng/mL medium (KO/DMEM/F12 supplemented with 1% (v/v) N2 supplement, 1 mM glutamine and 1% penicillin/streptomycin). The medium was changed every two days. bFGF was added every day to commit NSC into neuronal progenitor cells. At day 5 of differentiation, bFGF was removed and the cells were maintained for seven more days in N2 medium alone (again changed every two days). The cells were then cultivated in N2 medium containing laminin (1 ng/mL) and BDNF (10 ng/mL) until day 30 of differentiation. During this period, half of the media volume was refreshed every 3 days. Total media volume per well was 1 mL. The cells were treated (condition A: control medium containing DMSO (1/5000); condition B: ADAM10 inhibition with GI254023X (6 µM); condition C: HuPrP-directed 3F4 antibody [6 µg/well]; condition D: PrP-directed 6D11 antibody [6 µg/well]) at day 29 of differentiation and incubated for 18 h. Conditioned media and cells were then collected as follows: concentrated PI cocktail dissolved in 30

µL PBS was first filled in the collection tube (low-binding; Eppendorf) and conditioned media was carefully aspirated from the cell layer, added to the tube on ice and mixed by gentle inverting. Two mild centifugation of 5 min at 4 °C (500×*g*; 5000 × *g*) were performed to remove cell debris. For cell lysis, we freshly dissolved one tablet each of PI and PhosStop (Roche) in 8 mL of RIPA-Buffer. After carefully washing the cells on ice two times with cold PBS, 120 µL of this RIPA-Buffer were added, lysis was mechanically supported by scratching off the cells from the dish and pipetting up and down. Total duration of lysis was 20 min. Each sample (media and lysates) was stored at − 80 °C until analysis.

Human iPSC-derived cerebral organoids

Organoid generation and culture

Human induced pluripotent stem cell (iPSC) line KYOU-DXR0109B (ATCC) was routinely cultured on growth-factor reduced Matrigel (Roche) in mTeSR1 culture medium (StemCell Technologies) under standard incubator conditions (humidified, 37 °C, 5% CO_2). Cerebral organoids were generated from iPSCs using the STEMdiff cerebral organoid kit (StemCell Technologies) as per the manufacturer's instructions. For long-term culture they were maintained in cerebral organoid media (1 × glutamax, 1 × penicillin–streptomycin solution, 0.5 × non-essential amino acids, 0.5% (v/v) N2, 1 µL/4 mL insulin, 1% (v/v) B12 plus retinoic acid and 1 µL/286 mL β-ME in 1:1 Neurobasal:DMEM-F12 medium) on an orbital shaker at 85 rpm in a standard tissue culture incubator. This procedure was based on the protocol by [63].

Organoid imaging

Brightfield images of overall organoid morphology were captured using a Leica DMIL LED inverted microscope with a Leica HC 170 HD digital camera. Moreover, cerebral organoids were prepared for frozen sectioning by fixation in 10% (w/v) formalin for 24 h at room temperature (RT). Following washing in PBS, fixed organoids were incubated in 20–30% (w/v) sucrose for 24 h at RT, and then frozen at − 20 °C in optimal cutting temperature medium (Ted Pella Inc). For immunofluorescence (IF) stainings, slices were permeabilised in 0.1% (v/v) Triton-X-100 for 10 min, then blocked in 10% (v/v) FBS, 0.1% (w/v) BSA in PBS for 30 min before staining with primary antibodies in antibody buffer (1% (v/v) FBS, 0.1% (w/v) BSA in PBS) at the following dilutions: NF-L (Invitrogen) 1:50, OSP (Abcam) 1:50, FoxG1 (Abcam) 1:50, PrP SAF70 (Cayman Chemicals) 1:100, s100b (Abcam) 1:50. Secondary antibodies anti-rabbit-AlexaFluor-488 and anti-mouse-AlexaFluor-647 were diluted 1:250 in antibody buffer. Slides were mounted in Fluoromount-G Mounting Medium containing nuclear stain DAPI (Invitrogen). Images were captured using an EVOS FL Auto (Invitrogen) wide-field fluorescence microscope system.

Organoid treatments and sample harvesting

For experimental treatments, organoids were transferred into 24-well low adhesion plates (Corning) in 1 mL phenol red-free OptiMEM (Gibco) with reduced cerebral organoid media supplements (10% of routine culture concentrations) and the plates were incubated on the orbital shaker as for routine culture. For the GI254023X treatments (10 µM), organoids were pre-incubated with the compound for 2 h before changing media to fresh OptiMEM (already containing the compound) for 24 h. Anti-PrP 3F4 antibody and anti-mouse secondary antibody control (8 µg per well) treatments were set up in 100 µL of OptiMEM for one hour before diluting into the final media volume (1 mL) for 24 h.

Culture media collected from the treatments was supplemented with a 10 × concentrated solution of PI cocktail (Roche) at a 9:1 conditioned:fresh media ratio (i.e., 1 × final concentration of PI), then centrifuged at 500×*g* for 10 min at 4 °C to remove residual cell debris. Organoid lysates were made based on the wet weight of each organoid. Sufficient RIPA lysis buffer (Pierce) with 1 × PI was added to make a final 10% (w/v) homogenate and organoids were triturated. Conditioned media and lysates were stored at < − 20 °C until further assessment.

Biochemical methods

Trichloroacetic acid (TCA) precipitation

For the precipitation of proteins from cell culture supernatants, serum-free (OptiMEM) conditioned media of the overnight cultures were used. 10 µL (1/100 of vol.) of 2% sodium deoxycholate (NaDOC) was added to 1 mL sample and was shortly vortexed. After 30 min of incubation on ice, 100 µL (1/10 of vol.) of TCA (6.1N, Sigma) were added to each sample, vortexed and incubated again for 30 min on ice. Samples were then centrifuged at 15,000×*g* for 15 min at 4 °C. Next, the supernatant was entirely aspirated, and the pellet air-dried for 5 min and finally dissolved in 100 µL of 1 × SB containing β-ME. Due to remaining TCA and low pH, the blue SB turns yellow; for neutralization (and recovery of the blue color) 1.5 µL of 2 M NaOH were added and samples then boiled for 10 min at 96 °C.

Immunoprecipitation (IP)

Immunoprecipitation was carried out using dynabeads (Pierce Protein A/G Beads). Briefly, media from UW476 cells, cultured in OptiMEM for 48 h, was collected. After PI

addition, conditioned media was centrifuged first at 500×*g* and then at 5000×*g* (each for 10 min at 4 °C). The resulting supernatant was transferred to new tubes. Next, 750 µL aliquots of this supernatant were divided into different tubes, each receiving 7.5 µg of different antibodies (monoclonal V5B2 and polyclonal $sPrP^{Y226}$ for sPrP; monoclonal POM2 for total fl-PrP) or PBS (negative control). TCA-precipitated conditioned media was also added as a control for validating total sPrP amount. 40 µL of beads were washed with 200 µL of IP Lysis/Wash Buffer (provided in the kit). The antigen/antibody mixture was added to the beads and incubated for 2 h at RT in a rotator. Beads were magnetically immobilized to the tube wall and the supernatant (containing unbound proteins) was saved for analysis. Beads were washed twice with IP Lysis/Wash Buffer, followed by a wash with ultrapure water. Samples were then eluted with Elution buffer (kit content). To neutralize the low pH, Neutralization Buffer (kit content) was added. For WB analysis, 33 µL of 4 × SB (with 5% β-ME) was added to each sample, which was then boiled for 10 min at 96 °C.

Homogenisation of human and animal tissue samples

Frozen brain tissues from human and animals were used to prepare 10% (w/v) homogenates in RIPA buffer containing PI and PhosStop (Roche). Briefly, samples were homogenized either manually with 30 strokes in a dounce-homgenizer or using in-tube beads (Precellys) and incubated on ice for 15 min, prior to centrifugation at 12,000×*g* at 4 °C for 10 min. Total protein content was assessed by Bradford assay (BioRad). Homogenates were either further processed for SDS-PAGE (i.e., 30 µL of 10% homogenate + 120 µL of H_2O + 50 µL 4 × SB (containing 5% β-ME); denaturation at 96 °C for 10 min) or stored at − 80 °C. CSF samples were stored at − 80 °C, gently thawed on ice, mixed 1:3 with 4 × SB (containing 5% β-ME) and boiled for 10 min at 96 °C.

SDS-PAGE and western blotting

15–30 µL of denatured samples in SB (tissue homogenates, cell lysates, or precipitated conditioned medium) were loaded on precast Nu-PAGE 4 to 12% bis–tris protein gels (Thermo Fisher Scientific). After electrophoretic separation, wet blotting (at 200 mA per gel for 1 h) was performed to transfer proteins onto 0.2 µm nitrocellulose membranes (Bio-Rad). Total protein staining was performed according to the manufacturer's protocol (Revert™ Total Protein Stains kit; Licor). Thereafter, membranes were blocked for 45 min with either 1 × RotiBlock (Carl Roth) in Tris-buffered saline containing 1% Tween 20 (TBS-T) or 5% skimmed dry milk (dissolved in TBS-T) under gentle agitation at RT. Membranes were incubated overnight with the respective primary antibodies in the corresponding blocking reagents at 4 °C with gentle agitation. The following day, membranes were washed four times with TBS-T and incubated for 1 h at RT with either HRP- or IRDye-conjugated secondary antibodies (Licor). After several washes with TBS-T, membranes were developed [after incubating blots for 5 min with either Pierce ECL Pico or SuperSignal West Femto substrate (Thermo Fisher Scientific)] with a ChemiDoc imaging station (Bio-Rad) or were scanned using the Odyssey DLx imaging system (Licor). Densitometric quantification was done using the Quantity One software (Bio-Rad) and Image studio lite version 5.2 (Licor) followed by further analysis in Microsoft Excel and GraphPad Prism software.

(Immuno)histochemical stainings and immunofluorescence analyses

Immunohistochemistry (IHC)

Formaline-fixed paraffin-embedded (FFPE) brain tissues were used for immunohistochemical stainings. Samples from patients or animals with prion disease were incubated in formic acid (98–100%; duration depending on samples size) prior to embedding. Sections of 4 µm were prepared with a microtome and submitted to immunostaining following standard IHC procedures using a Ventana BenchMark XT machine (Roche Diagnostics). Sections were deparaffinated and underwent antigen retrieval by boiling for 60 min in 10 mM citrate buffer (pH 6.0). Afterwards, sections were incubated with primary antibodies diluted in 5% goat serum (Dianova, Hamburg, Germany), 45% TBS (pH 7.6), 0.1% Triton X-100 in antibody diluent solution (Zytomed, Berlin, Germany) for 1 h. Primary antibody (for further information refer to list above) dilutions were: V5B2 (1:50) or $sPrP^{Y226}$ (1:50), SAF84 (1:100, for PrP^{C} and PrP^{Sc}; note that for the latter (Fig. 6a) a harsh pretreatment with formic acid (5 min) followed by 30 min at 95 °C in 1.1 mM sodium citrate buffer [2.1 mM Tris–HCl and 1.3 mM EDTA (pH 7.8)], 16 min in PK and 10 min in Superblock was performed). Secondary antibody treatment was performed using anti-rabbit or anti-mouse Histofine Simple Stain MAX PO Universal immunoperoxidase polymer or Mouse Stain Kit (for detection of mouse antibodies on mouse sections). Detection of antibodies was done by Ultra View Universal DAB Detection Kit (brownish signals) or Ultra View Universal Alkaline Phosphatase Red Detection Kit (yielding pink signals) using standard machine settings (all solutions were from Ventana, Roche). Counterstaining (light blue background) was done according to standard procedures.

Stained sections were inspected, and representative pictures taken in TIF format on a digital microimaging device (DMD108, Leica) or with a Hamamatsu Slide Scanner and NDP.view2 software. The final picture processing for better presentation consisted of cropping, white balancing

(graduation curves; for IHC) and brightness adjustment (equally to all channels; for IF; see below) performed with Adobe Photoshop Elements 15 during figure assembly without affecting the findings and conclusions.

Immunofluorescence stainings of FFPE sections

Paraffin tissue sections were cut at 3 µm and thoroughly deparaffinized (2 × 20 min in Xylol and a descending alcohol row). Antigen retrieval was performed by boiling the sections in Universal R buffer (#AP0530-500; Aptum) for 20 min. Sections were briefly rinsed and blocked for 1 h. Antibodies against sPrP (1:100) and amyloid β (Aβ; 1:100; BAM-10 (Fig. 7c human sample) were incubated overnight at 4 °C. After intensive washing, AlexaFluor488- and AlexaFluor555-coupled anti-rabbit and anti-mouse secondary antibodies were applied for 1.5 h. Sections were washed again and mounted in DAPI-Fluoromount-G (SouthernBiotech). Data acquisition was performed using a Leica Sp5 confocal microscope and Leica application suite software (LAS-AF-lite).

The V5B2 epitope distribution in prion plaques (Fig. 6d, e) was studied using indirect IF on 5 µm-thick sections of FFPE cerebellar samples from patients with different prion diseases. Briefly, freshly deparaffinated sections were subjected to antigen retrieval, involving 30 min autoclaving at 121 °C in distilled water and 5 min incubation in 96% formic acid. After rinsing, 4% normal horse serum in buffer (block) was applied (20 min), followed by incubation with either V5B2 or 3F4 monoclonal antibody (at 20 µg/mL, overnight, at RT). Biotinylated horse anti-mouse secondary antibody (1:1,000, 90 min, Vector Laboratories) was applied, followed by incubation with streptavidin-Alexa 488 (1:750, 90 min, Molecular Probes). Next, fluorescence microscopy of single-labeled samples and image collection was performed, followed by second labeling: 4% normal donkey serum block was followed by V5B2 or 3F4 monoclonal antibody incubation (20 µg/mL, overnight, at RT). Signal detection was performed using Alexa 546-conjugated donkey anti-mouse secondary antibody (1:1000, 90 min, Molecular Probes). A Nikon Eclipse E600 fluorescent microscope equipped with appropriate filters (EX 465–695, DM 505, BA 515–555 and EX 528–553, DM 565, BA 590–650) and a Nikon DXM 1200 digital camera was used for fluorescence microscopy. Alternatively, Leica TCS confocal microscope (SP2 AOBS; Leica Microsystems) was used employing the 488 nm line of the Argon laser and 543 nm Helium–Neon laser excitation light through an acousto-optical beam splitter (Leica Microsystems). The emitted light was detected at 500–540 nm (green) and 543 nm (red) using spectrophotometer (SP2, Leica Microsystems). The excitation crosstalk was minimized by the sequential scanning. Images were processed using Leica confocal software.

IF staining of free-floating sections

Brains (Fig. 7c murine sample) were postfixed for another 4 h in 4% PFA (in PB) and then incubated in 30% (w/v) sucrose solution (in PB). After sinking down, brains were cut with a Leica 9000 s sliding microtome (Leica) into 35 µm thick free-floating sections. For IF staining, sections were incubated in blocking solution (0.5% Triton-X 100, 4% normal goat serum in 0.1 M PB pH 7.4) for 2 h at RT, followed by incubation with the primary antibody/antibodies (6E10 for human Aβ, LAMP1, $sPrP^{G227}$) in blocking solution at 4 °C overnight. Sections were washed three times with washing solution (0.1 M PB pH 7.4, 0.25% Triton X-100), incubated for 90 min in secondary antibody (in washing solution), washed two times again in the washing solution and one time in washing solution without Triton X-100. Finally, sections were mounted on glass slides, embedded in Mowiol (DABCO) and analyzed with a Zeiss LSM 980 fluorescence microscope equipped with an automated stage and the ZEN 3.3 software (Zeiss).

Brain vessel isolation and respective IF staining

Human brain microvessels were isolated as previously described [65]. The tissue was homogenized in 1 mL MCDB131 medium (ThermoFischer Scientific) using a dounce homogenizer, further diluted in medium and centrifuged (4 °C) at 2000×*g* for 5 min. The pellet was resuspended in 15% (w/v) 70 kDa dextran and centrifuged (4 °C) for 15 min at 10,000×*g*. The microvessel-containing pellet was retrieved and transferred to a 40 µm cell strainer. Isolated microvessels were fixed on the cell strainer with 4% PFA/PBS, retrieved in 1% BSA/PBS and centrifuged (4 °C) for 10 min at 2000×*g*. The pellet was dissolved in PBS and applied to Superfrost microscope slides. After air drying, the slides were stored at − 80 °C. Isolated 2D microvessels were stained with lectin GS-II (1:200), $sPrP^{Y226}$ (1:500) and 6E10 (1:200) or laminin (1:30), V5B2 and Thioflavin (1:200). High-resolution images were obtained with a Leica TCS SP8 confocal laser scanning microscope (Leica Microsystems) using a 63 × immersion oil lens objective.

Statistics

Student's *t* test has been applied for data presented in Figs. 4b and 7a (further information can be found in respective figure legends).

Results

Cleavage site prediction and targeted antibody production

Due to alterations in the C-terminal amino acid sequence between human and rodent PrP and lack of a glycine in a similarly membrane-proximate position as G227 (i.e. the P1 cleavage site and neo-C-terminus of sPrP in mice and rats [83, 122]), a different cleavage site for the shedding of human PrP was to be expected. Accordingly, our $sPrP^{G227}$ antibody previously generated for rodent sPrP [72] is ineffective towards the human protein. We therefore combined educated guessing and cleavage site prediction based on available sequence and structural data for human PrP (^{217}YERESQAYYQRGS^{230}) as potential substrate (Source: www.uniprot.org; Major prion protein [*Homo sapiens*], ID: P04156) and human ADAM10`s catalytic domain [114].

Although modeling the C-terminal sequence of PrP within the catalytic domain of ADAM10 is difficult (e.g., because of uncertainty regarding structural constraints imposed by PrP`s GPI- anchor), our modeling with PEPFOLD3 [125] and FlexPepDock [74] suggested the PrP tyrosine at 226 (Y226) as a possible P1 cleavage site within ^{217}YERESQAY^{226}↓QRGS^{230} (pink peptide), as shown by superposition with the enzyme-product complex of the C-terminus (^{642}FMRCRLVDADGPLG^{655}; yellow peptide) of adjacent ADAM10 subunits captured in the crystal structure of ADAM10 [114] (Fig. 1a (I and IV)). This conformation is possibly stabilized by R228 building a salt bridge with ADAM10`s E298 (Fig. 1a (II, III and V)) while ^{217}YERESQAYY^{226} (the conceivable C-terminal ending of newly formed sPrP) is being released from the catalytic center (Fig. 1a (IV)). Albeit PrP may not be regarded as an 'ideal' substrate (note that the vast majority of ADAM substrates are transmembrane proteins) and alternative cleavage sites would have been conceivable from a structural perspective, certain residues were in agreement with published cleavage site preferences identified with substrate libraries for recombinant ADAM10 using *quantitative proteomics for the identification of cleavage sites* (Q-PICS; [127]) or *terminal amine isotopic labeling of substrates* (TAILS [110];) (Fig. 1b). These data demonstrated that amino acid preferences of ADAM10 around the cleavage site slightly differ for peptide and protein substrates. Due to its GPI-anchor and N-glycans, mature cellular PrP exhibits additional molecular properties that certainly impact ADAM10 cleavage. Hence, although not in line with all 'most preferred' amino acids identified in the previous studies, cleavage of PrP by ADAM10 at Y226↓Q227 fits to residues A224 (in P3), Y226 (P1) and G229 (P3') (for PICS) as well as S222 (in P5) and G229 (P3′) (for TAILS), while no disfavored residues are present. Moreover, the distance of ~ 20 to 25 Å between the potential cleavage site and the plasma membrane (here mostly determined by PrP's GPI-anchor [77]) is in line with the membrane-proximity preferred by ADAM10 in complex with its regulator tetraspanin 15 [73] (which is involved in PrP shedding [115]).

Although neither us nor others [5, 83, 122] ever found indications of an involvement of the closely related ADAM17/TACE (with which ADAM10 shares several other substrates) in the C-terminal shedding of PrP, we also considered this metalloprotease and found some favored (A224 and G229 in PICS and TAILS, R228 in PICS) as well as disfavored PrP residues (Y225 and Q227 in PICS) (Fig. 1b).

Supported by these predictions and previous experience in raising cleavage site-specific antibodies for murine shed PrP [72], one of our groups generated antibodies against this putative shedding site, possibly enabling identification of extracellular PrP ending at Y226 as the physiologically relevant shed form (sPrP) in humans. Accordingly, rabbits were immunized with a respective peptide sequence and resulting polyclonal antibodies harvested and affinity-purified as described in the 'Materials and methods' section.

Confirming the ADAM10-dependency of PrP truncated at Y226 in human cell lines

Upon generation of polyclonal antibodies (termed $sPrP^{Y226}$) directed against this assumed neo-C-terminus (as done before for the murine system [72]), we first aimed at testing the banding pattern and ADAM10-dependency of immunoblot signals detected with this antibody. We also assessed any possible involvement of ADAM17/TACE in this supposed PrP shedding. We analyzed human lung carcinoma cells (A549) given their described decent expression levels of the relevant proteins [8, 49]. Molecular weight (MW) and glycoform pattern of bands detected with the $sPrP^{Y226}$ antibody in conditioned media were in line with earlier findings on murine sPrP [72] (Fig. 1c–f). Treatment with two metalloprotease inhibitors, GI254023X (with its much higher potency towards ADAM10 than ADAM17) and GW280264X (basically inhibiting both proteases) [45], alone or in combination, resulted in a lack of sPrP signal in conditioned media (Fig. 1c). While PrP shedding was completely absent upon GI treatment, this inhibitor had no effect on ADAM17 activity as judged by a previously reported postlysis autocatalytic processing step (i.e., mature ADAM17 cleaving itself into a slightly shorter fragment upon cellular breakup [111]) which was only inhibited in the presence of GW (Fig. 1c). In supposed contrast to PrP shedding, both proteases contribute to the non-amyloidogenic α-processing of APP as confirmed here by the differential

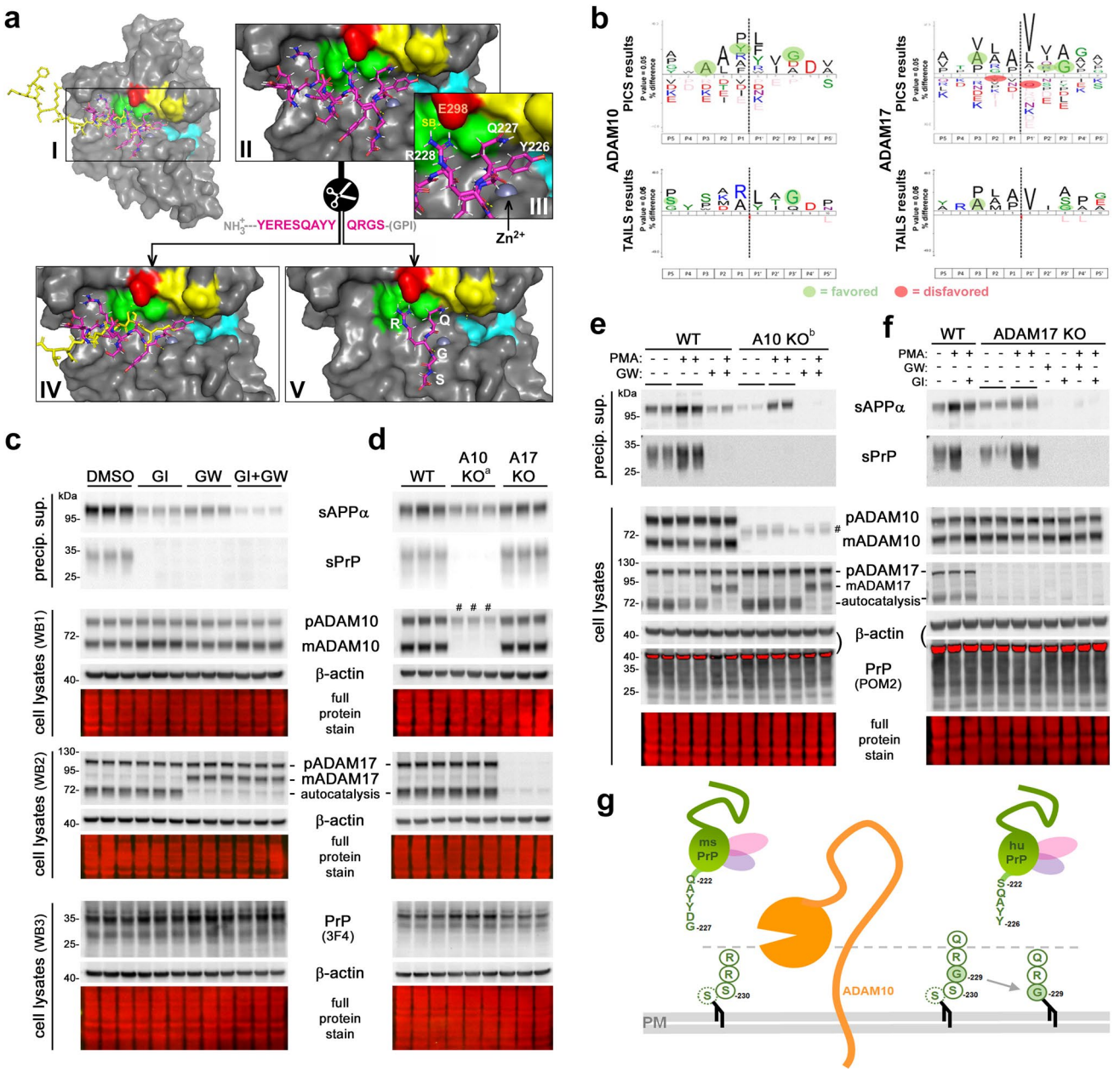

Fig. 1 Cleavage site prediction using structural models and pharmacological/genetic proof of human PrP shedding being ADAM10-dependent. **a** I: Proteolytic domain of ADAM10 (based on [114]) with Zn^{2+} coordinated in the catalytic center. Key residues of substrate-binding pockets highlighted for S1 (yellow; V297/F323/D325/V327), S1′ (cyan; V376/I379/T380/I416/T422) and S3 (green; L301/L330/W332). Overlaid extracellular C-terminal sequence ^{642}FMRCRLVDADGPLG^{655} (yellow) of another ADAM10 molecule (crystal structure PDB: 6BE6) and C-terminal end of PrP ^{217}YERESQAYYQRGS^{230} (purple). Magnification (II) and detail (III) of PrP's C-terminal sequence within ADAM10`s catalytic domain suggesting formation of a salt bridge (SB; PrP^{R228}-$ADAM10^{E298}$) and close proximity of the suspected cleavage site (Y226↓Q227) and Zn^{2+} within catalytic cave. IV: N-terminal parts (C-termini of sPrP or soluble ADAM10) are released after cleavage. V: Remaining C-terminal PrP residues may be freed from catalytic domain (possibly regulated by SB) and stay at the membrane or be endocytosed/degraded. **b** IceLogos: preferred and disfavored aa in different positions to the potential cleavage site (P1↓P1′) based on various peptide/protein substrates of ADAM10/ADAM17 using PICS (modified from [127]) and TAILS (modified from [110]). Favored (green background) and disfavored residues (red background) for putative PrP shedding. **c** WB of sPrP/sAPPα (media) and PrP/ADAM10/ADAM17 (lysates) of A549 cells treated with metalloprotease inhibitors GI254023X (GI) or/and GW280264X (GW). β-actin and total protein stain (TPS): loading controls. **d** Assessment in wild-type, ADAM10-knockout and ADAM17-knockout cells. **e** WB of WT and A10KO cells treated or not with ADAM-stimulating PMA and/or inhibitor GW. Two different A10KO lines were used (**d**: A10KO[a]; **e**: A10KO[b]; hence different inactive mutant bands #). **f** Analysis in WT and A17KO cells with/without PMA and/or GW/GI. Red saturated bands (**e**, **f**) result from residual β-actin signal (reprobing for PrP). **g** Model of membrane-proximate PrP shedding. With the recent suggestion of G229 (instead of previously assumed C-terminal serine) as actual GPI-attachment site in human PrP [51], distance between cleavage site and membrane would be preserved between mice and humans

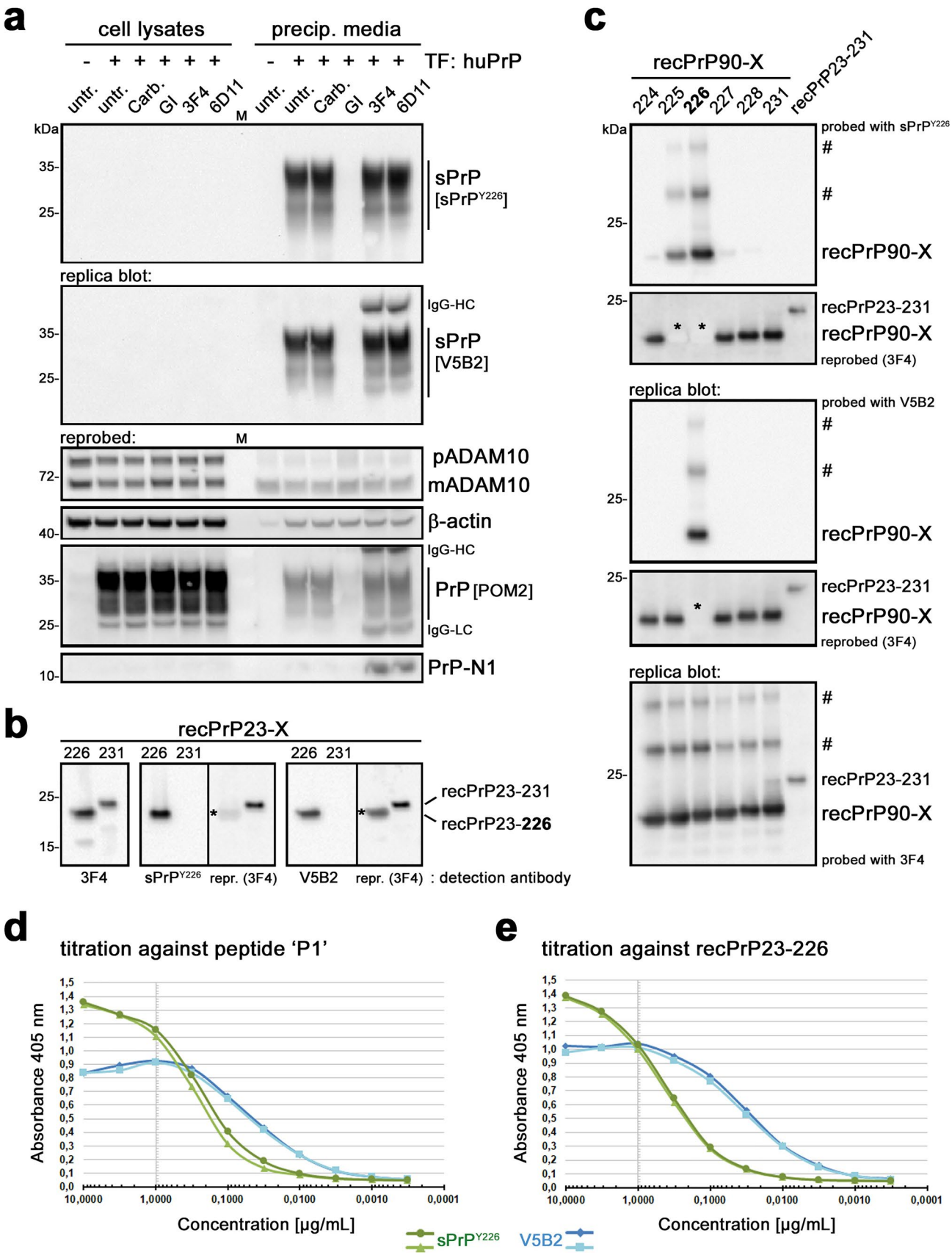
a
cell lysates
precip. media
TF: huPrP
untr. untr. Carb. GI 3F4 6D11 M untr. untr. Carb. GI 3F4 6D11
kDa
sPrP [sPrPY226]
replica blot:
IgG-HC
sPrP [V5B2]
reprobed:
pADAM10
mADAM10
β-actin
PrP [POM2]
IgG-LC
PrP-N1
b
recPrP23-X
226 231
recPrP23-231
recPrP23-226
3F4
sPrPY226
repr. (3F4)
V5B2
: detection antibody
c
recPrP90-X
224 225 226 227 228 231 recPrP23-231
probed with sPrPY226
recPrP90-X
recPrP23-231
reprobed (3F4)
replica blot:
probed with V5B2
probed with 3F4
d
titration against peptide 'P1'
Absorbance 405 nm
Concentration [µg/mL]
sPrPY226
V5B2
e
titration against recPrP23-226
Absorbance 405 nm
Concentration [µg/mL]

◂**Fig. 2** Direct comparison of polyclonal sPrP^{Y226} and monoclonal V5B2 antibodies. **a** Human neuroblastoma (SH-SY5Y) cells almost lacking endogenous PrP expression (see signal in lysates of non-transfected (−) cells; left lane) transfected (+) with a human PrP-coding plasmid, untreated (untr.) or treated with carbachol (Carb.), ADAM10 inhibitor GI, or PrP-directed antibodies 3F4 or 6D11. Cell lysates (left half of blots) and precipitated media supernatants (right half) loaded on two replica blots and initially detected with either sPrP^{Y226} or V5B2 yielding comparable signals (note that heavy chains (HC) of the treatment antibodies are also detected with the (anti-mouse) secondary antibody used for V5B2 detection). Re-probing with pan-PrP antibody POM2 confirmed overexpression of PrP in transfected cells (note that this cell-associated PrP was neither detected with sPrP^{Y226} nor with V5B2). Levels of premature (p) and mature/active (m) ADAM10, β-actin (loading control) and N-terminal PrP fragment N1 were also assessed. Actin in media indicates some transfection-induced cell death (note the comparably weak signal in untransfected cells). Dominance of mADAM10 in media likely associated with extracellular vesicles. Detectability of soluble PrP-N1 is rescued in the presence of 3F4 and 6D11 antibodies, protecting this instable fragment from proteolytic degradation [92]. M = marker lane. sPrP^{Y226} and V5B2 were also compared on replica immunoblots of recPrP23-226 (mimicking sPrP) versus recPrP23-231 (full-length) (**b**) or of N-terminally (i.e., at aa 90) truncated recPrP with different C-termini (X, as indicated) as well as full-length recPrP (23–231) (**c**). Blots were re-probed and an additional replica blot directly detected with the pan-PrP antibody 3F4. Asterisks in re-probed blots (**b** and **c**) mark "burned" signals resulting from overexposure during the previous detection shown above. '#' indicates SDS-stable dimers/oligomers of recPrP. Comparison of sPrP^{Y226} (green) and V5B2 (blue) in ELISA against the peptide 'P1' used for immunization of mice to generate V5B2 (**d**) or against human recPrP23-226 (**e**)

influence of respective inhibitors on sAPPα levels in media supernatants [41, 50, 60, 102]. These results were also confirmed in a human brain-derived glioblastoma cell line (U373-MG; Supplementary Fig. 1). However, considering the known cross-inhibition and imperfect 'specificity' of the metalloprotease inhibitors for particular ADAM members (i.e., GW also inhibiting ADAM10 activity), we further investigated A549 cells depleted via CRISPR-Cas9 in ADAM10 (A10 KO) or ADAM17 (A17 KO). This analysis revealed that a knockout of ADAM17 had no effect on levels of sPrP, whereas shedding was completely abolished in the absence of catalytically active ADAM10 (Fig. 1d). To further exclude that ADAM17 may only participate in PrP shedding at Y226 upon stimulation, we added the phorbol ester PMA, a widely used stimulus for ADAM17 activity, to WT and ADAM10 KO (Fig. 1e) or ADAM17 KO (Fig. 1f) A549 cells in the presence or absence of ADAM inhibitors. Although PMA treatment increased PrP shedding in WT cells, this effect was also observed in A17 KO cells, whereas no sPrP was detected in A10 KO cells. While this may support an influence of PMA on ADAM10 (e.g., via increased protein kinase C-mediated surface transport of ADAM10 [52]), the stimulated PrP shedding is clearly independent from ADAM17 expression. In sum, this analysis confirmed the strict dependence of the immunoblot signal obtained with the new sPrP^{Y226} antibody on ADAM10, supporting that Y226↓Q227 might indeed be the relevant shedding site in humans. It further suggested sole involvement of ADAM10 in this shedding event, as described earlier for rodents [5, 83, 122].

Notably, membrane interaction of the catalytic domain of ADAM10 and distance of cleavage sites within ADAM10`s substrates to the plasma membrane are relevant aspects for shedding to occur [73]. In this regard, it is intriguing that a recent study [51] suggested the GPI-anchor in human PrP being attached to glycine 229 (instead of the subsequent serine residues as previously assumed (Source: www.uniprot.org; Major prion protein [Homo sapiens], ID: P04156)), which would preserve a similar distance between membrane and shedding site as in mice (Fig. 1g).

Direct comparison of a poly- and a monoclonal antibody confirms PrP ending at Y226 as the product of ADAM10-mediated shedding in humans

Several years ago, one of our groups generated a set of mouse monoclonal antibodies against different C-terminally truncated forms of human PrP. Among those antibodies, one (termed V5B2) was described to specifically detect a shortened form of PrP ending at Y226 in the brains of a few patients suffering from prion disease [23, 27, 117, 128, 132]. The fragment was then designated PrP226* [54] and appeared to accumulate in prion aggregates and to even correlate with the spatial distribution of PrP^{Sc} deposits [75]. It was further characterized in vitro to predict structural and thermodynamic parameters affecting involvement in amyloid diseases [56, 58]. However, although the V5B2 antibody had been employed in several assays including ELISA, immunoblotting and immunohistochemistry (IHC), both the 'mechanistic' origin and physiological meaning of this fragment remained unclear until now, and there was no experimental support for it being a product of (physiological) ADAM10 proteolysis. We therefore directly compared the rabbit polyclonal sPrP^{Y226} antibody (introduced above) with the murine monoclonal V5B2 antibody. To this end, we first investigated the detection pattern of both antibodies in human neuroblastoma (SH-SY5Y) cells transiently transfected to overexpress human PrP (given the very low endogenous levels shown in the non-transfected control) (Fig. 2a). Two replica blots, both containing cell lysates and respective precipitated media supernatants, were first probed with either sPrP^{Y226} or V5B2 antibody. Both yielded very similar signals only in media samples of transfected cells yet not in respective cell lysates, and no signal was detected in media of cells treated with the ADAM10 inhibitor. When reprobed with the pan-PrP antibody POM2, strong overexpression of PrP in the lysates of transfected cells was confirmed. This overexpression may explain the lack of further elevated sPrP levels

upon treatment with either Carbachol (a drug normally able to increase PrP shedding as shown in Supplementary Fig. 2 and reported elsewhere [47]) or PrP-directed IgGs known to stimulate shedding [71], as endogenous ADAM10 might simply be 'saturated' by the artificially high levels of PrP. In sum, both sPrP^{Y226} and V5B2 yield highly comparable WB signals, specifically detecting human ADAM10-cleaved shed PrP while being "blind" for its cell-associated full-length 'precursor'.

Next, we analyzed the specificity of the antibodies against recombinant PrP variants ending at either position 231 or Y226. While a pan-PrP antibody detected both forms, polyclonal sPrPY226 and monoclonal V5B2 antibodies only detected the truncated recPrP ending at Y226 (Fig. 2b). We then wondered about the epitope tolerance of both antibodies and assessed their ability to detect different C-terminally truncated versions of human recPrP90-X by western blotting. For a cleavage site-specific monoclonal antibody, one would expect one exclusive signal for PrP90-226, whereas an analogue polyclonal antibody (due to its potential 'repertoire' of different IgGs) could conceivably also provide signals for fragments with neighboring C-terminal endings. Our analyses exactly confirmed this assumption as monoclonal V5B2 solely detected recPrP90-226, whereas polyclonal sPrP^{Y226} also detected few other fragments, albeit with much lower sensitivity (Fig. 2c). However, since such fragments likely do not exist in nature (despite the possibility of some rare stop mutations), the polyclonal sPrP^{Y226} antibody—like the monoclonal V5B2—can be regarded as a bona fide cleavage site-specific detection tool for human sPrP. Both antibodies also revealed bands at higher molecular weight likely representing SDS-stable oligomers of respective recombinant PrP variants.

To further examine sPrP binding propensity of V5B2 and sPrP^{Y226}, we compared their relative binding affinities (RBA; i.e., concentration of the antibodies at half of the saturation, expressed in moles, M = mol/L) with ELISA. We performed titration experiments either against peptide 'P1' (CITQYERESQAYY, used for V5B2 generation [23, 132]) (Fig. 2d) or against recombinant human PrP ending at Y226 (recPrP23-226) (Fig. 2e). Despite slight differences in the curves, both antibodies showed a relatively high affinity with resulting RBAs against 'P1' of 2.0×10^{-10} (V5B2) and 1.0×10^{-9} (sPrP^{Y226}) and against recPrP23-226 of 1.3×10^{-10} (V5B2) and 1.3×10^{-9} (sPrP^{Y226}). This further supports their overall similar binding characteristics and usability in various methodological approaches. However, we also noted that the polyclonal antibody might be slightly better suited for detection of sPrP in denatured samples (as indicated by immunoblot comparison on serial dilutions of human brain; Supplementary Fig. 3), whereas its monoclonal pendant might be superior for native samples (as suggested by the ELISA results and a better performance in immunoprecipitating sPrP from conditioned cell culture media; Supplementary Fig. 4).

Ligand-induced shedding of PrP in human cells

We have previously shown in the murine system that treatment of cells and brain slice cultures with certain PrP-directed antibodies stimulates the ADAM10-mediated shedding in a substrate-specific manner [71]. Moreover, as shown above and earlier [72], shedding is completely abolished with an ADAM10 inhibitor. To investigate if these manipulations also work in the human neural system, and to further confirm that PrPY226 indeed corresponds to genuine, physiologically shed PrP, we employed these paradigms to three human brain-derived cancer cell lines which we had screened before for relevant endogenous expression of both ADAM10 and PrP. In our previous study using murine cells and tissues, 6D11 (an antibody binding to a central region in PrP) caused highest shedding among the PrP ligands tested, whereas the 3F4 antibody served as a negative control (as its epitope is absent in murine PrP yet present in human PrP). In the human cancer cell lines SHEP2 (neuroblastoma-derived; Fig. 3a), LN235 (astrocytoma-derived; Fig. 3b) and U373-MG (glioblastoma-derived; Fig. 3c), both antibodies—as expected—stimulated the shedding when compared to controls (albeit with only moderate effects of 6D11 in SHEP2 cells). Moreover, as shown before in mice, shedding of diglycosylated PrP seems to be preferred over the other glycoforms (as judged by comparison with the PrP glycopattern in respective lysates). In further agreement with murine samples and fitting to the lack of the GPI-anchor and the very C-terminal amino acids, sPrP bands run at a slightly lower molecular weight than PrP in lysates. Besides a different ratio of premature and mature ADAM10 between the cancer cell lines (Fig. 3a–c), no obvious differences in PrP or ADAM10 levels were observed in cell lysates upon treatments.

With regard to the shedding-stimulating effect of PrP-directed antibodies, our previous study on murine samples revealed one striking exception: POM2 IgG, an antibody directed against four repetitive epitopes along the flexible N-terminal tail of PrP, instead of increased shedding rather causes a general reduction in PrP levels in both cell lysates and corresponding media supernatants. This is due to clustering and multimerization at the cell surface triggering internalization and lysosomal degradation [71]. Here, we also addressed this aspect and found the PrP-reducing effect of POM2 in the three human cell lines investigated (Fig. 3d).

Together with the complete inhibition of shedding with the ADAM10-specific inhibitor in all three cell lines of neural origin (Fig. 3a–c), these data strongly support both, (i) Y226 being the relevant cleavage site for ADAM10 in human PrP and (ii) our PrPY226-directed antibodies

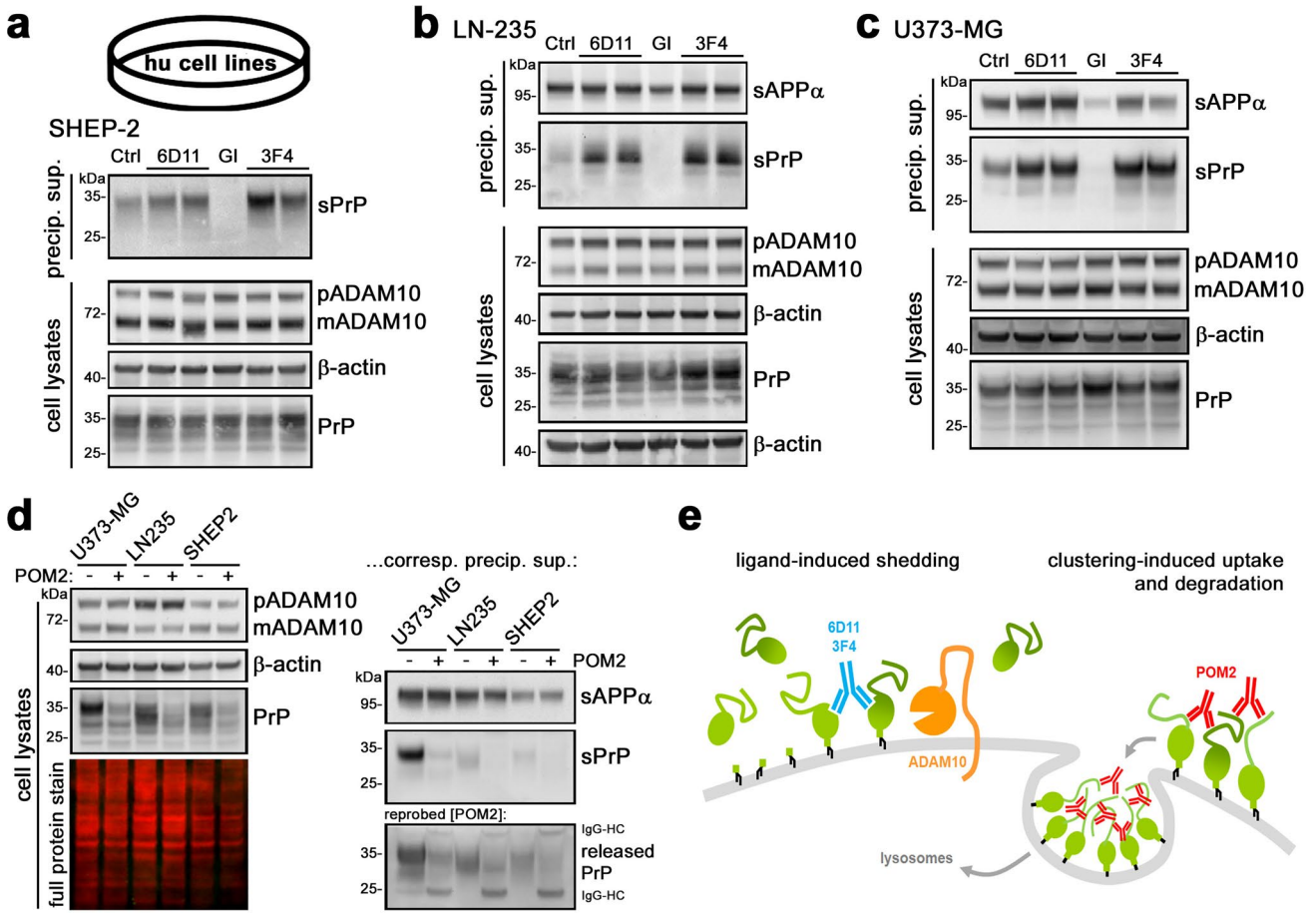

Fig. 3 PrP shedding, ADAM10 inhibition, and effects of PrP-directed antibodies in human CNS cancer cell lines. Representative WB showing basal levels of sPrP (Ctrl; left lane of each blot) detected with the $sPrP^{Y226}$ antibody in precipitated overnight media supernatants of neuroblastoma cells (SHEP-2; in **a**), astrocytoma cells (LN-235; in **b**) and glioblastoma cells (U373-MG; in **c**). In all cell lines, shedding is increased upon treatment with PrP-directed antibodies 6D11 and 3F4 and abolished when treated with an ADAM10 inhibitor (GI). sAPPα was detected in media (in **b** and **c**) as another cleavage product generated by ADAM10. Corresponding cell lysates assessed for levels of PrP, premature (p) and mature/active (m) ADAM10, and β-actin (serving as loading control) are shown underneath (**a**–**c**). **d** Treatment with the antibody POM2 in all three cell lines results in the reduction of cell-associated PrP levels (left panel) as well as sPrP and released PrP in corresponding media samples (right panel). **e** Scheme showing the shedding-stimulating effect of PrP-directed antibodies and the exceptional reduction in total PrP levels caused by POM2 IgG (illustration modified from [71])

specifically detecting endogenously generated shed PrP. Moreover, the shedding-stimulating effect of PrP-directed antibodies as well as the downregulation of total PrP levels caused by POM2 IgG (both illustrated in Fig. 3e) are reported here for the first time in a human paradigm.

Depletion of EVs lowers sPrP in conditioned media yet also allows for the use of pan-PrP antibodies to support PrPY226 as the relevant and ADAM10-dependent shed form

In earlier EV-related experiments, we occasionally noted a reduction of sPrP in conditioned media upon ultracentrifugation, and we thought this is likely due to binding of sPrP to EVs (see model in Supplementary Fig. 5a). In this regard, homophilic interaction with GPI-anchored PrP on EVs, binding to other surface receptors or association with the EV membrane or corona components are conceivable. As mentioned earlier, assessment of sPrP with classical pan-PrP antibodies is difficult due to exceeding amounts of full-length PrP (especially on EVs) of almost similar molecular weight (scheme in Supplementary Fig. 5b). Thus, EVs have to be depleted from a given sample. To this end, we ultracentrifuged conditioned media of U373-MG cells. A substantial reduction of sPrP and total PrP in supernatants was confirmed while sPrP appeared in the dissolved EV pellet (Supplementary Fig. 5c). Upon ADAM10 inhibition, sPrP was neither found in the soluble nor in the pelleted fraction. Next, we performed ultracentrifugation and deglycosylation (to avoid confusing bands due to different PrP glycoforms) in

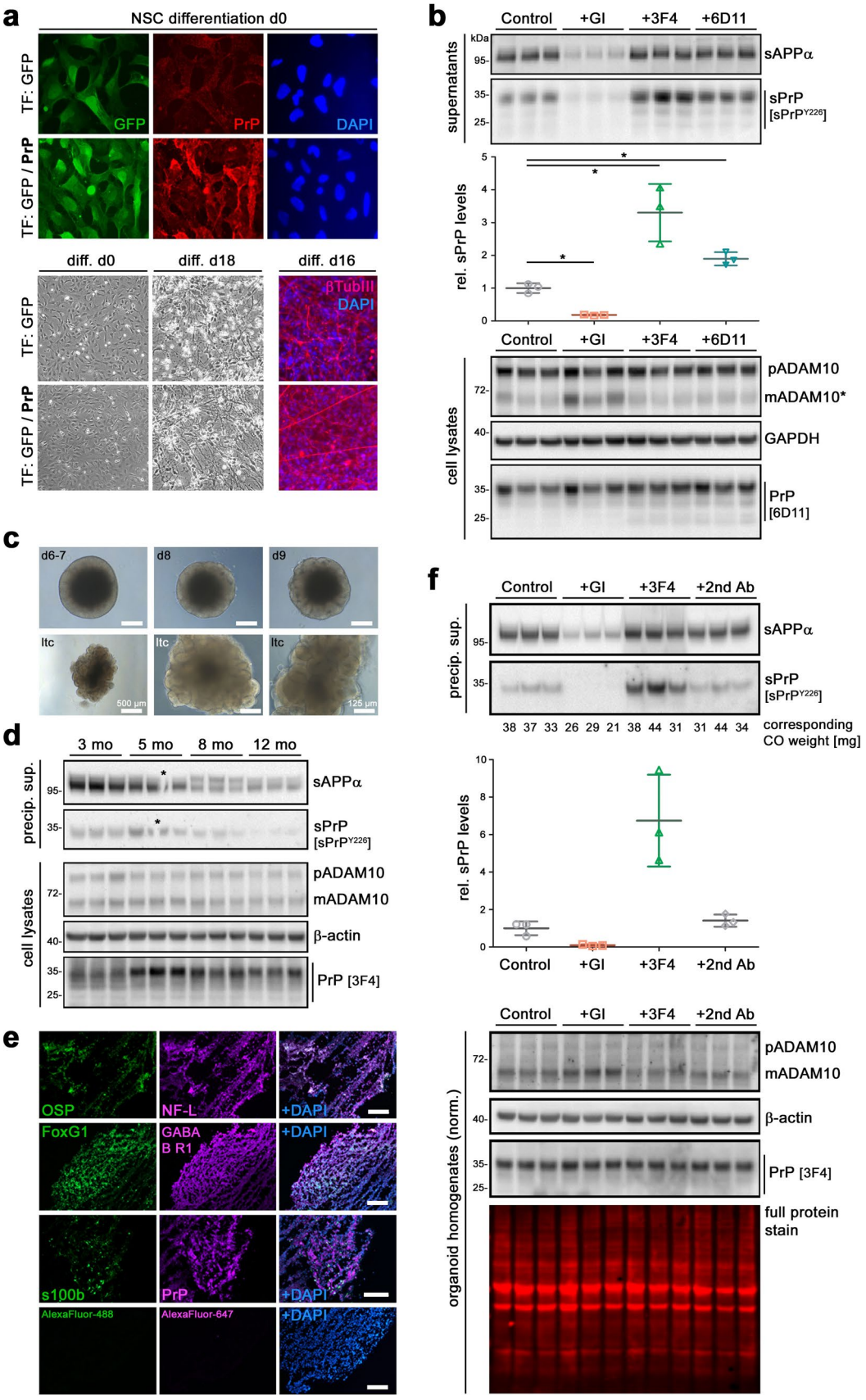
a
NSC differentiation d0
TF: GFP
TF: GFP / PrP
GFP
PrP
DAPI
diff. d0
diff. d18
diff. d16
βTubIII
DAPI
b
Control
+GI
+3F4
+6D11
supernatants
kDa
95-
35-
25-
sAPPα
sPrP
[sPrPY226]
rel. sPrP levels
cell lysates
72-
40-
pADAM10
mADAM10*
GAPDH
PrP
[6D11]
c
d6-7
d8
d9
ltc
500 µm
125 µm
d
3 mo
5 mo
8 mo
12 mo
precip. sup.
sAPPα
sPrP
[sPrPY226]
cell lysates
pADAM10
mADAM10
β-actin
PrP [3F4]
e
OSP
NF-L
+DAPI
FoxG1
GABA B R1
s100b
PrP
AlexaFluor-488
AlexaFluor-647
f
Control
+GI
+3F4
+2nd Ab
precip. sup.
sAPPα
sPrP
[sPrPY226]
38 37 33 26 29 21 38 44 31 31 44 34
corresponding CO weight [mg]
rel. sPrP levels
pADAM10
mADAM10
β-actin
PrP [3F4]
organoid homogenates (norm.)
full protein stain

◂**Fig. 4** PrP shedding in human neuronally differentiated stem cells and iPSC-derived cerebral organoids. **a** IF analysis of embryonic stem cell-derived NSC (upon lentiviral transfection to express either GFP (green) or GFP and exogenous PrP (red)) at day 0 of neuronal differentiation (upper panel). Bright field microscopy (lower left panel) showing morphological differences between day 0 and 18. IF analysis at day 16 (lower right panel) reveals neuronal marker β-tubulin III. **b** Immunoblot of sPrP and sAPPα in conditioned media (supernatants; upper panel), quantification of relative sPrP levels (diagram; middle panel), and cellular levels of ADAM10, GAPDH and PrP (lysates; lower panel) following 30 days of differentiation and 18 h treatment with ADAM10 inhibitor GI (a lower concentration [6 µM] was used here, hence the residual signal for sPrP) or PrP-directed IgGs (3F4/6D11). DMSO-treated controls served as reference (set to 1). $n=3$ wells per condition; mean ± SE; Student's t test with $^*p<0.05$. **c** iPSC-derived cerebral organoids (CO) at different days of differentiation and after neuroepithelial bud expansion ready for long-term culture (ltc). Scale bar 250 µm unless indicated. **d** Levels of sPrP and sAPP (conditioned media) and PrP, ADAM10 and β-actin (loading control) in CO homogenates after 3–12 months in culture. **e** Different cell types detected in differentiated organoids by IF analysis of typical markers (OSP = oligodendrocyte-specific protein; NF-L = neurofilament light chain (neurons); GABABR1 = γ-aminobutyric acid type B receptor subunit 1 (inhibitory neurons); s100b = S100 calcium-binding protein B (astrocytes)). PrP expression was also detected. DAPI used to stain nuclei. Controls with only fluorescently labeled 2nd antibodies (AlexaFluor) revealed no signals. Scale bars 200 µm. **f** Treatment of CO with GI (inhibition), 3F4 antibody (stimulation) and a non-specific secondary antibody (negative control). sPrP and sAPP in precipitated media (sPrP quantification shown below) and ADAM10 and PrP in respective CO homogenates (individual CO weights shown below lanes) assessed by WB. TPS and β-actin: loading controls. We refrained from statistical analysis considering variation in CO weights

media of cells treated with shedding-stimulating antibodies (or co-treated with ADAM10 inhibitor GI). As expected, only one clear band (lower than 25 kDa) was detected with our cleavage site-specific antibody (Supplementary Fig. 5d), and the signal was increased upon treatment of cells with 6D11 or 3F4 antibodies, whereas it was absent in cells receiving 6D11 and GI, once again supporting ADAM10 dependency. Importantly, immunoblot detection with pan-PrP antibodies 3F4 or EP1802Y did not reveal any additional bands (one would expect if alternative cleavage sites in the vicinity would exist) than those identified as PrPY226. Lastly, we performed a similar analysis in A549 WT and ADAM10 KO cells stimulated (or not) with PMA (Supplementary Fig. 5e). Although sPrP signals, compared to Fig. 1c–f, were substantially reduced and rather difficult to detect (especially in non-stimulated conditions) due to the EV depletion, we confirmed increased PrP shedding with PMA in WT cells. Again, no sPrP was detected in ADAM10 KO cells, although PMA also stimulated the alternative α-secretase ADAM17 (as indicated by increased sAPPα production). Notably, immunoblot detection with 3F4 antibody did not uncover fragments other than the $sPrP^{Y226}$-positive ones. In sum, these experiments suggest that cleavage site-directed antibodies allow for the reliable detection of "real" sPrP levels in a biological sample without the need for prior EV depletion. Moreover, using pan-PrP antibodies for detection of sPrP upon ultracentrifugation of conditioned media, we found no support for alternative proteolytic cleavages in the far C-terminal region of PrP that would qualify as "physiological shedding". This, however, does not exclude the possibility of other processes contributing to PrP release under certain conditions (e.g., cleavage of the GPI-anchor structure by phospholipases).

Manipulation of PrP shedding in human neuronally differentiated embryonic stem cells and iPSC-derived brain organoids

Having confirmed in different human cell lines that PrP ending at Y226 is identical with physiological proteolytically shed PrP in humans, we directly assessed its presence and pattern in more complex cellular systems of human origin. Human neural stem cells (NSC) transduced to coexpress GFP (as a reporter) and PrP (due to low endogenous levels) were differentiated into a neuronal lineage (Fig. 4a). Cultures were then treated to manipulate the ADAM10-mediated shedding of PrP (as done before in cell lines). While treatment with the ADAM10 inhibitor impaired the shedding, PrP-directed antibodies 3F4 and 6D11 caused increased levels of sPrP in conditioned media (Fig. 4b). We next investigated this in human iPSC-derived cerebral organoids (Fig. 4c). After 5 months of culture, expression levels of ADAM10 and PrP were highest (Fig. 4d, quantifications in Supplementary Fig. 6), sPrP was detectable in conditioned media (Fig. 4d), and diverse brain cell types (except for microglia) constituted the organoid as confirmed by expression of typical markers (Fig. 4e). We therefore chose this stage for treatment experiments. Again, shedding of PrP was abolished upon GI-treatment, whereas it was increased upon incubation of cells with the 3F4 antibody binding to human PrP (Fig. 4f).

Heterologous cleavage occurs, and the new cleavage site-specific antibodies also detect shed PrP of animal species susceptible to naturally occurring prion diseases

Given the difference in C-terminal sequence and shedding sites between human and rodent PrP, we wondered whether heterologous cleavage (i.e., human ADAM10 shedding mouse PrP and vice versa) is possible. To this end, we first expressed human PrP in murine PrP-depleted N2a cells [92]. Replica blots of the same conditioned media were probed either with our polyclonal antibody for rodent sPrP ($sPrP^{G227}$) or with the respective counterpart for human sPrP ($sPrP^{Y226}$) (Fig. 5a). A similar experiment was done including both murine and human PrPs with a GFP tag in

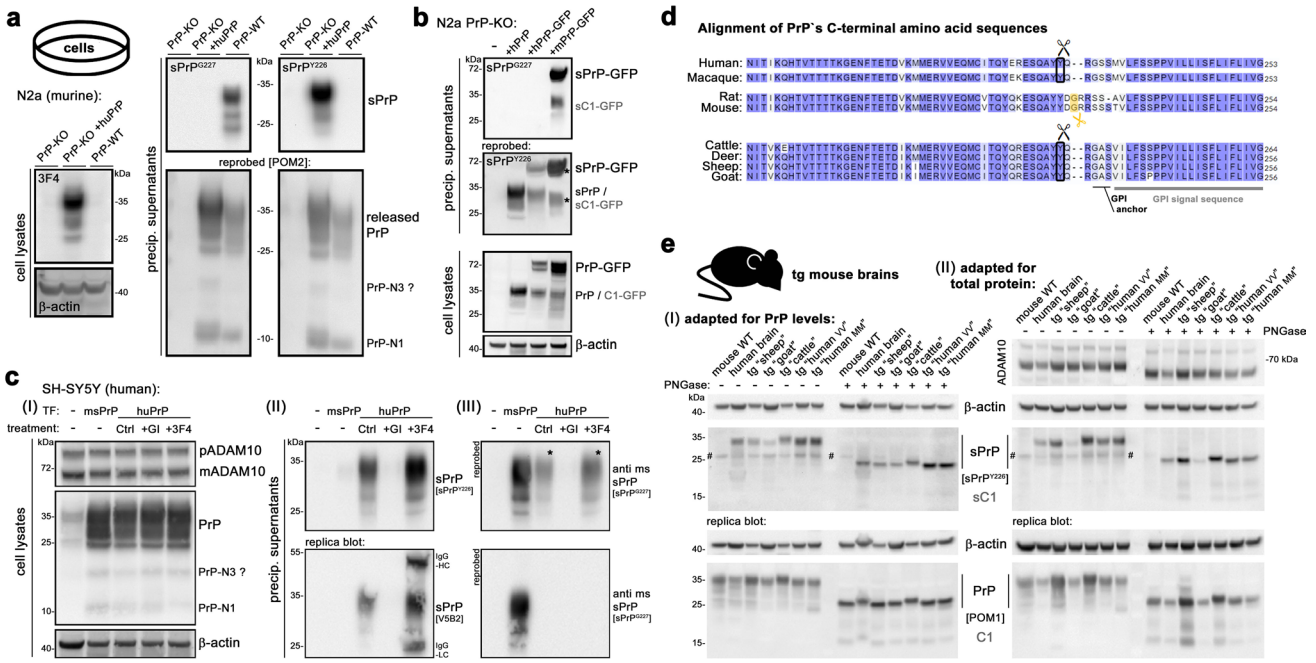

Fig. 5 Heterologous cleavage and species-specificity of sPrP-directed antibodies. **a** Shedding in murine (ms) PrP-KO N2a cells overexpressing human (hu) PrP (PrP-KO and WT-N2a were controls for no and endogenous PrP expression, respectively). HuPrP overexpression confirmed by a 3F4-positive signal. Replica blots of precipitated media detected with either $sPrP^{G227}$ (ms sPrP) or $sPrP^{Y226}$ (hu sPrP). Presence of released PrP fragments was confirmed by re-probing with POM2. **b** WB of PrP-KO cells transfected with huPrP or GFP-tagged versions of hu or ms PrP (GFP located within the C-terminal half of PrP). $sPrP^{G227}$ exclusively detects ms sPrP-GFP and shed C1-GFP, whereas re-probing with $sPrP^{Y226}$ reveals hu sPrP, sPrP-GFP and shed C1-GFP in media samples. Expression of respective cell-associated PrP forms in lysates (using pan-PrP antibody POM1) shown below. **c** WB of hu SH-SY5Y cells transfected (TF) with msPrP or huPrP (the latter treated or not with GI or 3F4-IgG). (I) Lysates; (II) replica blots of precipitated media probed with either polyclonal $sPrP^{Y226}$ (top) or monoclonal V5B2 (bottom) detecting hu sPrP (basal (Ctrl), inhibited (GI) or increased (3F4)); (III) re-probing with $sPrP^{G227}$ reveals ms sPrP (* indicates signals from the initial detection due to primary/secondary antibody combination). **d** C-terminal aa sequences of PrP in different species including GPI-anchor signal sequence and attachment site. The ADAM10 cleavage site is marked in yellow for rats and mice, in black for human and monkey PrP. Note the sequence similarity of the latter with cattle, deer, sheep and goat. **e** Assessment of sPrP and PrP in brains of transgenic (tg) mice expressing PrP of different species. WT mouse and a human brain homogenate included as controls. PNGase F digestion performed for deglycosylation (shown on the right side of each blot). Protein amounts were either roughly adapted to PrP expression (I) or normalized for total protein (II). Actin: loading control, ADAM10 levels are also shown in II. # indicates an unspecific band detected with $sPrP^{Y226}$

their C-terminal domains (Fig. 5b). Shedding occurred in all instances, indicative of ADAM10 being tolerant to other species sequences and preserving those PrPs cleavage sites. Similar results were obtained when expressing murine PrP in human SH-SY5Y cells (Fig. 5c). These experiments also further support the specificity of the different sPrP-directed antibodies. Moreover, detection of N1 (and N3) (in Fig. 5a and c) and C1 fragments (in Fig. 5b) indicates that α-cleavage (and γ-cleavage), for which responsible proteases are not yet identified without doubt, also occur in a heterologous setting. Next, we assessed whether antibody $sPrP^{Y226}$ raised against human sPrP would also detect sPrP in other species. Upon initial analyses of CNS samples from a broad range of domestic and zoo animals, we got a glimpse of some promising fragments (fitting to either sPrP or the shed N-terminally truncated C1 fragment) not only in human and macaque, but also in goat, sheep, cattle and two deer species (Supplementary Fig. 7). Fittingly, the latter species, in contrast to mice and rats, largely share the sequence around the cleavage site in human PrP (Fig. 5d). This prompted us to perform further analysis in transgenic mice (depleted for endogenous PrP) expressing PrP from either sheep, goat, cattle or human PrP (the latter with MM or VV status at polymorphic position 129). Using the $sPrP^{Y226}$ antibody, sPrP forms were detected in the brains of all transgenic mice (Fig. 5e). This not only confirms the heterologous cleavage discussed above, but also reveals that PrP shedding in those major species prone to naturally occurring prion diseases (i.e., scrapie in sheep and goats; BSE in cattle, and CWD in deer) occurs after the respective tyrosine corresponding to Y226 in the human sequence. Here again, we directly compared the performance of both sPrP antibodies in some of these transgenic mice (versus WT and PrP-KO mice) by immunoblotting (Supplementary Fig. 8). This analysis

supported similar overall detection profiles, yet also confirmed that the polyclonal version reveals stronger signals when detecting denatured samples.

Altered distribution of sPrP with accumulation in extracellular deposits uncovers presence of PrP^{Sc} aggregates in different human and animal prion diseases

Some cases of human prion diseases are linked to *PRNP* stop mutations causing expression of pathogenic C-terminally truncated (and hence anchorless) PrP versions, which form large extracellular and often vessel-associated deposits. Notably, normal (i.e., non-genetically truncated) PrP expressed by the unaffected allele associates with these aggregates [34, 35, 84, 100]. But why and how should regular membrane-anchored PrP actually end up in plaques to a relevant extent? Since we recently showed in prion-infected mice that sPrP co-localizes with bona fide PrP^{Sc} deposits [71], we considered the aforementioned findings in patients may either reflect passive recruitment of sPrP to PrP^{Sc} deposits or even an active involvement of the shed form in extracellular sequestration of harmful oligomeric PrP^{Sc} assemblies. To address whether this interaction might be a more widespread phenomenon, we performed morphological assessment to directly assess tissue distribution of sPrP and its potential association with prion deposits in brain samples of human and—given the detection characteristics of our antibodies—animal prion diseases. As shown in Fig. 6a, in a control brain not diagnosed with neurodegeneration, sPrP appears uniformly like a background staining due to its diffuse and even distribution. In prion diseases, however, sPrP (using polyclonal $sPrP^{Y226}$) becomes visible and, even without a harsh pre-treatment required for detection of bona fide resistant PrP^{Sc}, indicates presence of extracellular prion aggregates both in sporadic CJD (sCJD) cases of the MM2C type (coarse-grained and perivacuolar deposits in the cortex) and the MV2K type (Kuru-like plaques in cerebellum), reminiscent of our earlier findings in mice [71]. In cerebellum of the MV2K case, sPrP clusters were even more pronounced than actual PrP^{Sc} plaques, which may suggest a role as an aggregation hub for oligomeric misfolded proteins. Re-localization and aggregate association of sPrP was also observed when monoclonal V5B2 was used to stain brains affected by sCJD or variant CJD (Fig. 6b). A direct comparison of both antibodies (Supplementary Fig. 9) confirms a comparable detection pattern of $sPrP^{Y226}$ and V5B2 in different sCJD subtypes and brain regions. Since cattle and sheep share the cleavage site (Fig. 5), we stained brain samples of these species affected or not by classical BSE and classical scrapie, respectively, and again found the sPrP-characteristic re-distribution in the presence of prion deposits (Fig. 6c). Immunofluorescence analysis of different human prion diseases (vCJD and Gerstmann–Sträussler–Scheinker (GSS) syndrome in Fig. 6d and sCJD in Fig. 6e) further revealed the intimate association of sPrP with prion plaques. Lastly, since heterologous shedding occurs (Fig. 5), we assessed transgenic mice expressing either ovine PrP (tg338, infected or not with NPU1 prions; Fig. 6f and Supplementary Fig. 10a, b) or bovine PrP (with or without vCJD infection; Fig. 6g and Supplementary Fig. 10c). Besides confirming the aforementioned partial colocalization of sPrP with the respective strain-characteristic extracellular prion deposits in different brain regions, we also found a pronounced vessel-associated pattern.

Shed PrP also closely associates with extracellular amyloid deposits in AD and is readily detectable in human CSF

In AD and other neurodegenerative diseases, large deposits of disease-associated misfolded proteins may be less harmful than their diffusible synapto- and neurotoxic oligomeric states [38, 43, 62, 131, 133]. Earlier studies reported presence of PrP within Aβ deposits in AD brain [13, 31, 36, 121], yet the mechanistic origin of this plaque-associated PrP remained obscure until our recent demonstration in mouse models that this particularly identifies as sPrP [71, 93]. This finding, together with the capacity of soluble PrP fragments to bind and detoxify Aβ [18, 33, 95, 113] and the known ability of PrP to foster Aβ aggregation [29, 112], suggest a protective sequestration of Aβ (and possibly other harmful PrP-binding extracellular oligomers alike) driven by sPrP. When analyzing sPrP levels in AD brain at different disease stages by WB, we found interindividual differences yet no significant alterations between groups (Fig. 7a), fitting to similar total amounts of sPrP detected earlier in brains of 5xFAD mice and controls [71]. A moderate increase in ADAM10 levels was noted in our samples with higher disease stage (Supplementary Fig. 11). Upon immunohistochemical assessment of sPrP, similar to our findings in the presence of prion deposits (Fig. 6), we observed a marked redistribution into structures reminiscent of larger diffuse deposits or smaller dense plaques of Aβ, which was absent in non-AD controls (Fig. 7b). Occasionally, we also found dense deposits associated with vessels in brains of patients with AD and those without diagnosed neurodegenerative disease. Immunofluorescence co-stainings in AD samples then revealed enrichment of sPrP in amyloid plaques, as seen before in mouse models for Aβ pathology (Fig. 7c) [71, 93]. When isolating microvessels from AD brain, in some instances extracellular plaques were co-purified and showed an intimate association between Aβ and sPrP (Fig. 7d). Moreover, this analysis also confirmed presence of sPrP in vessel-associated amyloid deposits (Fig. 7d and e; orthogonal views shown in Supplementary Fig. 12). Lastly,

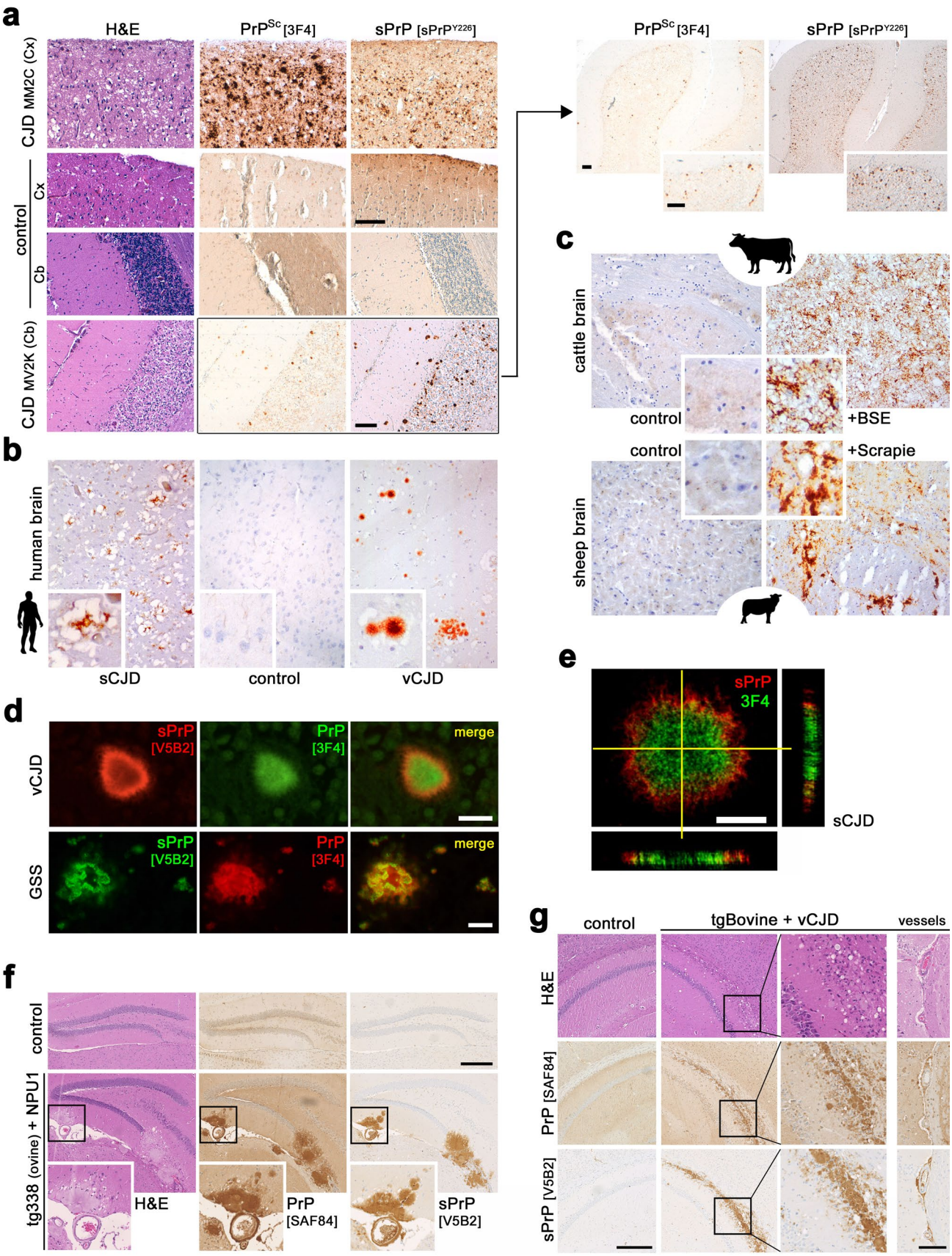
a
H&E
PrP^Sc [3F4]
sPrP [sPrP^Y226]
CJD MM2C (Cx)
control
Cx
Cb
CJD MV2K (Cb)
b
human brain
sCJD
control
vCJD
c
cattle brain
control
+BSE
+Scrapie
sheep brain
d
vCJD
GSS
sPrP [V5B2]
PrP [3F4]
merge
e
sPrP
3F4
sCJD
f
control
tg338 (ovine) + NPU1
H&E
PrP [SAF84]
sPrP [V5B2]
g
control
tgBovine + vCJD
vessels
H&E
PrP [SAF84]
sPrP [V5B2]

◂**Fig. 6** Redistribution of sPrP and association with prion deposits in prion diseases of humans and animals. **a** (Immuno)histochemical (IHC) assessment of PrP^{Sc} (3F4 antibody upon harsh tissue pre-treatment) and sPrP (polycl. antibody $sPrP^{Y226}$) in two CJD cases compared to a control without diagnosed neurodegeneration. Coarse-grained and perivacuolar PrP^{Sc} deposits present in frontal cortex [Cx] of a MM2C case, while the cerebellum [Cb] of a MV2K case shows typical Kuru-like plaques (note that tissue disruption in control is due to pre-treatment prior to PrP^{Sc} detection). Shed PrP shows a diffuse distribution in the control and re-distributes into an aggregated appearance in brains affected by CJD (scale bars 100 µm). In MV2K, more sPrP clusters appear than actual PrP^{Sc} plaques, which is further supported by an overview comparison (upper right panel). **b** Monocl. antibody V5B2 used in IHC to detect sPrP in brain sections of a sCJD and a vCJD patient (compared to a control). **c** Detection of sPrP (V5B2) in the brains of cattle affected or not with BSE (upper panel) and sheep with or without Scrapie (lower panel). **d**, **e** IF analyses showing association of sPrP (V5B2) with extracellular PrP aggregates (3F4) in acquired (vCJD) and genetic prion diseases (GSS) (**d**; standard fluorescence microscopy; scale bars 20 µm) and sCJD (**e**; z-stacks with side projections; scale bar 5 µm). **f**, **g** Histological analyses of large PrP^{Sc} deposits (here: SAF84 antibody without harsh pre-treatment) and sPrP (V5B2) in hippocampal areas of prion-infected transgenic mice expressing ovine (tg338; **f**) or bovine PrP (**g**). Tg338 mice infected with NPU1 prions present with large and dense amyloid-like plaques (**f**). TgBov mice infected with vCJD show extended prion deposition along the corpus callosum. Boxes indicate position of magnified areas (**g**). In both models, association of aggregates with brain vessels is observed. Non-infected mice of the respective genotype served as controls. Scale bars 250 µm (and 100 µm for the 'vessels' panel in **g**)

we addressed detectability of sPrP in human CSF. When adjusted to balance total protein content, both sPrP and shed C1 (sC1; resulting from PrP α-cleavage followed by ADAM10-mediated shedding) were much more abundant in CSF than in brain homogenates (Fig. 7f), fitting to a soluble factor being drained into body fluids [120].

Thus, sPrP closely interacts with aggregating proteins associated with human neurodegenerative diseases. Since sPrP seems to be immobilized inside deposits of misfolded proteins and may hence be kept inside the brain in respective pathologies rather than being physiologically drained into the CSF, further studies addressing conceivable disease-related alterations in sPrP levels in body fluids are warranted regarding a diagnostic potential.

Discussion

New pathomechanistic insight and potential therapeutic targets together with earlier diagnosis are urgently required in the field of currently incurable neurodegenerative diseases, ranging from rather rare transmissible prion diseases to Alzheimer`s disease, the most frequent cause of dementia. Focusing on the proteolytic processing of PrP, a common denominator in these conditions of the brain [3, 21, 22, 25, 30, 36, 64, 96, 103, 105, 123] and potentially relevant player in other pathophysiological processes throughout the body [7, 78, 79, 81, 86, 93, 101, 135], we here formally demonstrate that ADAM10 is the physiological sheddase of PrP in humans, mediating the release of nearly full-length PrP from the plasma membrane. We identified its cleavage site in humans (and some mammalian species most relevant for natural animal prion diseases) and present cleavage site-specific antibodies allowing to detect sPrP with a variety of techniques and in different biological samples. We also provide the first demonstration that human brain sPrP, usually diffusely distributed in the extracellular space, is relocalized in the presence of extracellular deposits of misfolded proteins, closely associating with the latter. While this may support a protective sequestrating activity of sPrP towards toxic protein assemblies, it confirms earlier findings in mouse models [71, 93] and provides a mechanistic rationale for the widespread earlier observation of "normal PrP" being enriched in extracellular protein deposits in diverse human proteinopathies [13, 31, 34–36, 84, 97, 100, 121]. A scheme summarizing the key findings is provided in Fig. 8.

The interest in endogenous proteolytically generated PrP fragments is steadily increasing [6, 19, 24, 55, 59, 130] with more and more functions and pathological implications being suggested, particularly for 'sPrP' [7, 78–81, 86, 101]. Yet due to the lack of appropriate tools, most studies either did not sufficiently discriminate between sPrP and other released PrP forms (e.g., on EVs) or drew their conclusions from experiments using synthetic PrP, considering the latter to be a suitable analogue for physiological sPrP. This may or may not be the case (given the potentially relevant differences in glycosylation state and C-terminal ending [93]). Cleavage site-specific antibodies, now available for rodents [72] and the human system (as presented here), will certainly be valuable in clarifying these and future questions.

With regard to neurodegenerative diseases, promising PrP-related therapeutic strategies include reduction of total or cell surface PrP levels (e.g., via antisense oligonucleotides (ASOs) [91, 94, 104] or other compounds [87]) and treatment with PrP-directed antibodies or other ligands (aiming to block membrane-bound PrP`s interaction with toxic conformers and/or to stabilize its native fold [85] (reviewed in [71])). Our previous identification in murine samples of a ligand-stimulated shedding of PrP [71] adds another mode of action, linking both concepts and likely contributing to protective effects ascribed to PrP-binding antibodies. Enabled by our sPrP-specific antibodies used for detection, we here show that this mechanism also applies to the human context. Though speculative at the moment, combination therapies are conceivable. A PrP expression-lowering approach, for instance, could be combined with stimulated shedding to "transform" the remaining (likely harmful)

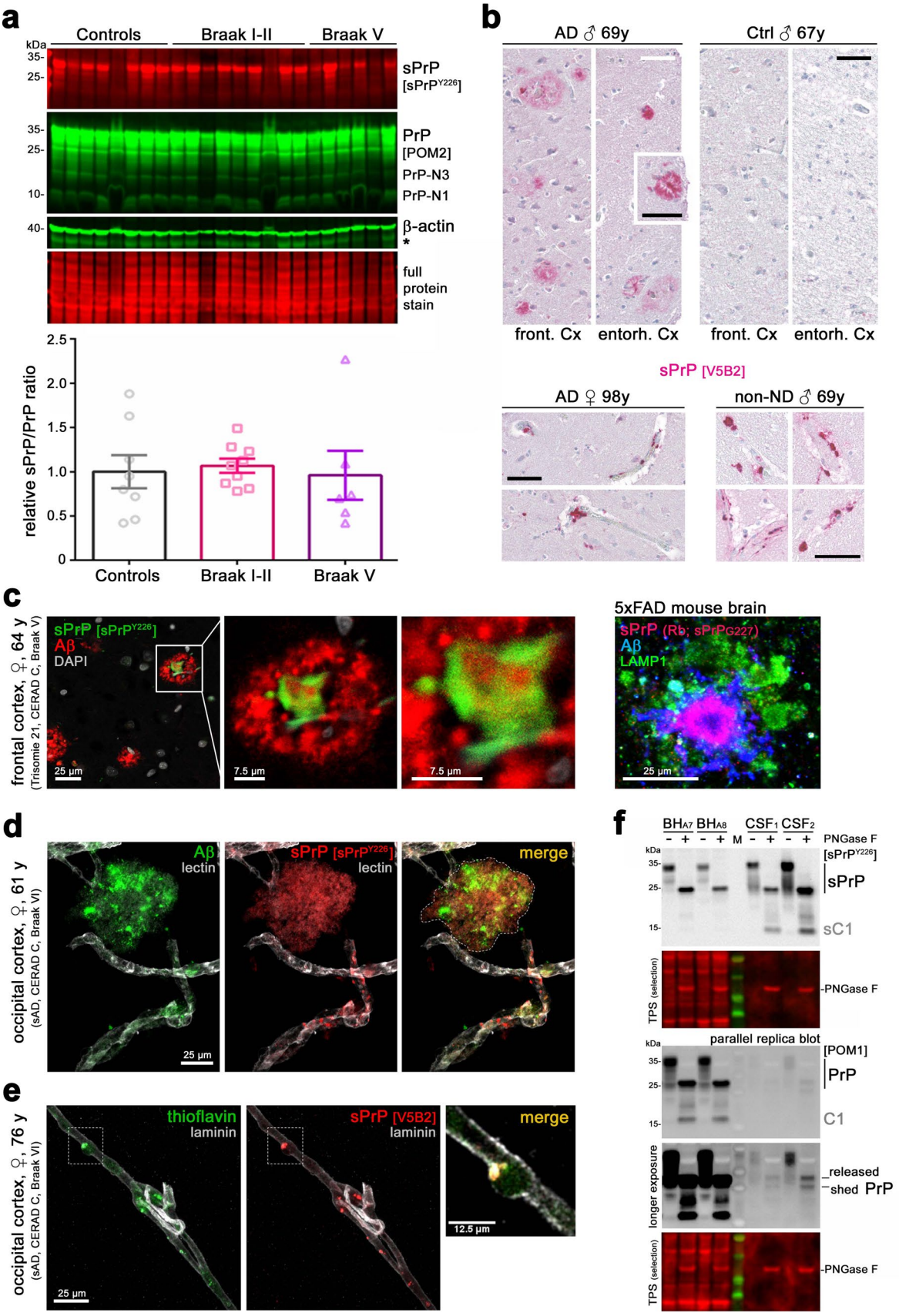
a
Controls
Braak I-II
Braak V
kDa
35-
25-
sPrP
[sPrP^Y226]
35-
25-
10-
PrP
[POM2]
PrP-N3
PrP-N1
40-
β-actin
*
full
protein
stain
relative sPrP/PrP ratio
2.5
2.0
1.5
1.0
0.5
0
Controls
Braak I-II
Braak V
b
AD ♂ 69y
Ctrl ♂ 67y
front. Cx
entorh. Cx
front. Cx
entorh. Cx
sPrP [V5B2]
AD ♀ 98y
non-ND ♂ 69y
c
frontal cortex, ♀, 64 y
(Trisomie 21, CERAD C, Braak V)
sPrP [sPrP^Y226]
Aβ
DAPI
25 µm
7.5 µm
7.5 µm
5xFAD mouse brain
sPrP (Rb; sPrPG227)
Aβ
LAMP1
25 µm
d
occipital cortex, ♀, 61 y
(sAD, CERAD C, Braak VI)
Aβ
lectin
sPrP [sPrP^Y226]
lectin
merge
25 µm
e
occipital cortex, ♀, 76 y
(sAD, CERAD C, Braak VI)
thioflavin
laminin
sPrP [V5B2]
laminin
merge
25 µm
12.5 µm
f
BHA7
BHA8
CSF1
CSF2
- + - + M - + - +
PNGase F
kDa
[sPrP^Y226]
35-
25-
15-
sPrP
sC1
TPS (selection)
-PNGase F
parallel replica blot
kDa
[POM1]
35-
25-
15-
PrP
C1
longer exposure
released
shed PrP
TPS (selection)
-PNGase F

◂**Fig. 7** Shed PrP analysis in AD and CAA, and sensitive detectability of sPrP in human CSF. **a** WB analysis of sPrP and total PrP in cortex of AD patients (Braak stage I–II ($n=8$), Braak stage V ($n=9$)) compared to non-neurodegeneration controls ($n=6$). Actin and TPS: loading controls. Asterisk indicates signals from previous PrP detection. Besides inter-individual alterations in sPrP, quantification (below) of the sPrP/PrP ratio reveals no significant differences between groups. **b** IHC of sPrP in AD and controls with sPrP showing both diffuse and dense (birefringent) plaque-like pattern reminiscent of bona fide Aβ deposits (upper panel). Dense vessel-associated sPrP signal can be found in some AD cases and controls (lower panel). Scale bars 50 µm. **c** Closer inspection by IF microscopy in brain sections of a patient with AD/Trisomy 21 reveals sPrP in the center of some (yet not all) Aβ plaques, as reported earlier in mouse models ([71]; on the right: sPrP detection in 5xFAD brain with $sPrP^{G227}$ antibody; LAMP1 indicates dystrophic neurites or microglial lysosomes). **d** Plaque-like clusters (highlighted by dotted line in merge picture) of Aβ and sPrP co-purified during isolation of microvessels from AD brain. Co-localization of both molecules was also found at/in vessels. Lectin: endothelial marker. Orthogonal projection of this picture presented in Supplementary Fig. 9a). **e** Association of amyloid and sPrP in/at brain vessels was verified in another AD case using another set of stainings (V5B2 for sPrP, thioflavin for (Aβ) aggregates, anti-laminin as endothelial/vessel marker). Another vessel of this sample shown in orthogonal view in Supplementary Fig. 9b). Scale bars as indicated. **f** WB of sPrP and total PrP in brain homogenates (BH) and CSF samples (patients not diagnosed with neurodegeneration). Deglycosylation (+PNGase F) performed for better detection of (shed) C1 fragment (resulting from shedding after α-cleavage). 20 µg of protein were loaded for BH, whereas CSF samples had only 1 or 3 µg of total protein

membrane-bound PrP into a released (possibly protective) anchorless factor (while conceivably even preserving physiological ligand functions of sPrP).

PrP levels in body fluids not only serve as disease biomarker [26, 89], but also as a surrogate marker for treatment efficacy, e.g. in ASO-based PrP-lowering strategies [90, 129]. However, "PrP" in this context rather represents a pool of different iso- and proteoforms [70, 130] and, in addition, is enriched on certain EV subtypes [16, 72]. A compensatory network connects mechanisms of cellular PrP processing and release [72], yet how production of the different PrP forms is regulated and how it would react to manipulation of PrP expression is unknown. Available pan-PrP antibodies, depending on their epitopes, would either not discriminate between diverse differentially regulated and affected PrP subforms or could be unresponsive for some of the latter. Reliable detection of a well-defined fragment, such as sPrP, and treatment-associated alterations therein could therefore be superior, highlighting a conceivable diagnostic potential of the cleavage site-specific antibodies presented here [90, 126, 129].

Reliable surrogate markers are critical when it comes to pharmacological targeting of highly disease-relevant enzymes such as secretases [17, 37, 68]. The rather ubiquitous expression of both ADAM10 and PrP in different organs, cell types and experimental models, and the current view that no other proteases (such as ADAM17) seem to be involved in PrP shedding, may suggest a potential of measuring sPrP as a surrogate marker for efficacy read-out in any experimental or therapeutic strategies targeting ADAM10, be it stimulation of its protective APP α-secretase activity in the context of AD or inhibition of its rather detrimental effects, e.g. in cancer and inflammatory diseases [107]. Hence, future studies aiming to manipulate ADAM10 may take advantage of sPrP-specific antibodies in basic research and clinical trials. However, assessing ADAM10-mediated cleavages remains complex, since this protease is regulated at various biological levels (transcription, translation, transport, membrane dynamics, maturation/activity, extracellular matrix modulation, etc.) and multiple players (e.g., interaction partners of both substrate and protease, exact subcellular localization, substrate availability/competition, endogenous stimulators/inhibitors), and activity towards one substrate in a given context or sample does not necessarily correlate with activity towards another one [17]. Whether sPrP qualifies as a reliable read-out in a given context needs to be evaluated.

We are only starting to understand the (patho)physiological roles played by sPrP. Further mechanistic studies are clearly required to investigate if and how sPrP indeed supports sequestration of toxic proteopathic oligomers into respective deposits, and whether its interaction with those conformers in the extracellular space may induce additional effects (such as receptor binding and cellular uptake for degradation or activation of glial responses). The relevance of Aβ-associated sPrP in brain vessels also deserves a more detailed investigation. Likewise, whether stimulated shedding—at least partially—contributes to the protective effects of certain PrP-directed antibodies in current therapeutic approaches (and clinical trials [85]) against prion diseases remains to be investigated. Whether or not sPrP, as a soluble factor drained into body fluids, such as CSF and blood, holds potential as an easily accessible diagnostic biomarker, as a reliable reporter for treatments targeting PrP expression, or even as a read-out for any ADAM10-targeting strategies in various pathophysiological processes certainly requires detailed and careful examination and is currently being investigated. The sPrP-specific antibodies characterized herein lay the foundation for these and other initiated and follow-up investigations.

But is it appropriate to only discuss sPrP in the context of (neuro)protective aspects? This conclusion would probably be premature and not satisfying the actual complexity. Recent reports suggest a role of sPrP in the development and drug resistance of certain human tumors [101, 135] while others have proposed a detrimental role in neuropathological complications caused by HIV infection [86]. Regarding the latter, "soluble PrP" was found increased in body fluids of HIV patients with neurocognitive impairment [106], suggesting that our sPrP-specific antibodies could foster new

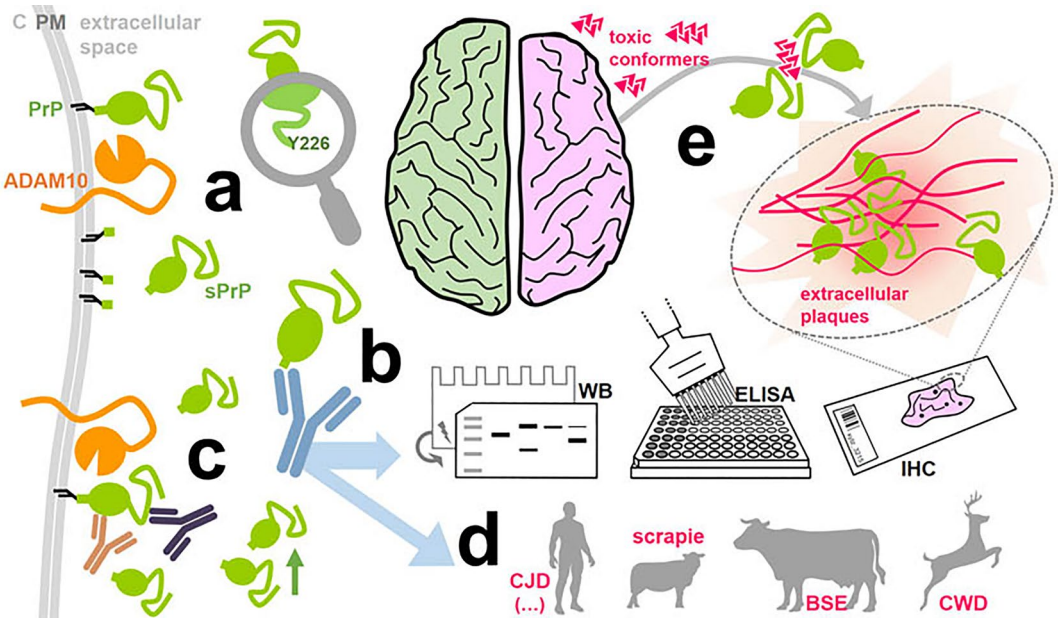

Fig. 8 Graphical summary of sPrP-specific antibodies and PrP shedding in humans*. **a** The widely expressed metalloprotease ADAM10 (orange) is the functionally relevant sheddase of PrP (green) in the human body and constitutively releases shed PrP (sPrP) into the extracellular space, from where it is also drained into body fluids such as CSF (not depicted to simplify matters). C = cytoplasm; PM = plasma membrane. We here identified the cleavage site between PrP's tyrosine 226 and glutamine 227. **b** We generated cleavage site-specific antibodies against this neo-C-terminus (Y226). The sPrP-specific poly- and monoclonal antibodies do not detect full-length membrane-bound forms of PrP and can now be used in several routine methods, such as immunoblotting (WB), ELISA, and immunohistochemistry (IHC), to analyse a wide range of biological samples in basic science and diagnostics. **c** As shown before in mice, we demonstrate that PrP shedding can also be stimulated in the human system by PrP-directed ligands (e.g., antibodies), a mechanism of potential therapeutic value. **d** *We also found that the cleavage site in human PrP is shared by other mammals including sheep/goats, cattle and deer. Hence, the sPrP-specific antibodies presented here will also foster analyses in the most relevant species (naturally) affected by prion diseases. **e** Among other findings, we show that sPrP redistributes from a diffuse pattern (in healthy brain) to markedly cluster with extracellular deposits of misfolded proteins in neurodegenerative diseases of humans and animals, possibly pointing towards a protective sequestrating activity of sPrP (containing all relevant binding sites) against toxic diffusible conformers in the extracellular space

systematic insight with regard to pathomechanisms and diagnostic potential beyond the field of protein misfolding diseases. It is tempting to speculate that these instances may be connected with the known harmful upregulation of ADAM10 in tumorigenesis, metastasis and inflammatory conditions [107].

And what about prion diseases? In murine disease models (and possibly dependent on the actual prion strain under investigation), aggregates of misfolded PK-resistant yet ADAM10-cleaved forms of PrP ($sPrP^{res}$) were shown in recent studies using our sPrP-specific antibody for mouse samples [1, 116]. This fits earlier reports showing that misfolded PrP can, in principle, be released from cells by ADAM10 (yet, remarkably, not by phospholipases cleaving within the GPI-anchor structure) [15, 118, 122]. Alternatively, shed PrP could undergo misfolding in the extracellular space, similar to what was shown in transgenic mice expressing anchorless PrP [20, 119]. Notably, although ADAM10 expression in prion-infected transgenic mice appeared to correlate with reduced overall prion conversion and longer survival (indicative of reduced PrP-associated neurotoxicity) [4, 28, 93], histological assessment pointed towards ADAM10 supporting spatiotemporal spreading of neuropathological hallmarks within the brain [4]. This dual role fits the previously described mechanistic uncoupling of prion formation/infectivity on the one hand, and neurotoxicity on the other hand (with the latter primarily being determined by cell surface PrP^{C} levels and defining disease tempo) [10, 109]. Thus, possibly depending on prion strain and the affected species, $sPrP^{res}$ (or 'shed prions') may also contribute to prion spread inside and outside an organism. In this regard, it will be particularly interesting to study whether 'proteolytic shedding' and potential presence of $sPrP^{res}$ in saliva, nasal secretions, urine or feces of deer and elk contributes to the efficient 'environmental shedding' and, hence, horizontal transmission of prions causing highly contagious CWD [11, 82, 124]. Detailed investigations on the role of shedding in naturally occurring prion diseases in humans and other relevant mammals are certainly warranted and will profit from the findings and research tools presented herein.

In conclusion, following cleavage site-prediction and generation/characterization of respective site-specific antibodies, we have provided strong evidence that PrP shedding in humans at position Y226 is orchestrated by ADAM10 and can be stimulated in a substrate-targeted manner. Shedding at the corresponding position also occurs in other mammalian species affected by prion diseases. Using our site-specific antibodies, sPrP is readily detectable in CSF (maybe holding biomarker potential), and an altered distribution of sPrP in brain (possibly affecting its drainage into body fluids) is seen in neurodegenerative diseases with extracellular protein deposits, indicative for a sequestrating activity of sPrP towards toxic misfolded proteins. While this might reflect a protective feature of blocking toxic oligomers extracellularly in some conditions (e.g., in AD), the consequences of PrP shedding might be more ambivalent in prion diseases (where 'anchorless misfolded PrP entities' potentially involved in disease spreading and transmission, and maybe representing bona fide 'prions' are generated by ADAM10). All of these aspects as well as roles of the ADAM10-mediated PrP release in physiological and disease conditions in various tissues certainly need to be studied in greater detail. Our sPrP-specific antibodies hold great promise to fundamentally support such investigations and enable novel critical insight.

Supplementary Information The online version contains supplementary material available at https://doi.org/10.1007/s00401-024-02763-5.

Acknowledgements We thank Kristin Hartmann, Edda Thies, and Celina Soltwedel as well as the Mouse Pathology Core and the Microscopy Imaging Facility 'UMIF' (all at UKE Hamburg, Germany), and Bradley Groveman (NIH Hamilton, USA) for excellent technical assistance. N2a cells depleted for PrP (PrP-KO) were kindly provided by Dr. Michael Willem (LMU, Munich, Germany) and LN235 cells by Prof. Dr. Monika E. Hegi (University of Lausanne, Centre hospitalier universitaire vaudois, Epalinges/Lausanne, Switzerland). Some human brain tissue samples were kindly provided to BTCS (upon completion of diagnostic procedures and full anonymization) by Prof. Dr. Mara Popović (Institute of Pathology, University of Ljubljana, Slovenia), Prof. Dr. Herbert Budka (Medical University Vienna, Austria) and Prof. Dr. James Ironside (National CJD Surveillance Unit, University of Edinburgh, UK). We also thank R-Biopharm (Darmstadt, Germany) for providing V5B2-stained human, sheep and cattle brain images (in the framework of a former Collaboration Agreement with BTCS).

Author contributions Performed experiments/investigation and/or analyzed datasets: FSo, VK, BM, JLL, FSch, AM-A, IV, MSha, GG, SD, LL, MC, KH, SK, STF, CM, CLH, HCA. Provided critical research tools, samples, infrastructure and ideas, and/or supervised individual experiments, scientific discussion: SJ, JT, JN, MD, SKT, SFL, FLR, TS, MSch, IZ, BP, ET, IF, TM, MSR, DS-F, JM, LMS, MB, OA, RN, CB-P, CC, CLH, MG, VCS, HCA. Visualization/final figure assembly: HCA. Conceived and designed this study, literature research, project administration, funding, supervision, and wrote the manuscript: HCA. All authors contributed to, commented on and/or edited the manuscript. All authors read and agreed on the content of the manuscript.

Funding Open Access funding enabled and organized by Projekt DEAL. This research was kindly supported by the*CJD Foundation Inc., USA, theAlzheimer Forschung Initiative(AFI) e.V., Germany, and theWerner-Otto-Stiftung, Germany (all to HCA),Deutsche Forschungsgemeinschaft(DFG) CRC877 "Proteolysis as a regulatory event in pathophysiology" (project A12 to MG), DFG under Germany's Excellence Strategy (EXC) within the framework of theMunich Cluster for Systems Neurology(EXC 2145 SyNergy—ID 390857198 to SFL), DFG (TA 167/6-3 and EXC 2033—390677874 – RESOLV to JT), DFG (SCHA 2248/2–-1 to FSch),China Scholarship Council(grant #202108080249 to FSo),Slovene Research Agency(grant numbers: L3-3435, L3-6006, L3-0206, P4-0176, P3-0171 and PhD student funding), CLH and STF are funded by the intramural research program of NIAID (NIH, USA), AMA's contributions were supported by the European Union'sHorizon 2020research and innovation program (through the Marie Skłodowska Curie grant agreement #101030402).*

Availability of data and materials All relevant datasets used and/or analyzed during the current study are presented in the manuscript. Additional data will be available from the corresponding authors on request. The authors will be happy to provide the cleavage site-specific antibodies directed against shed PrP and characterized herein as research tool upon reasonable request.

Declarations

Conflict of interest The authors have no conflict of interest to declare.

Ethics approval Use of human and animal samples was in agreement with respective international and institutional guidelines as well as local regulations. This work was covered by respective approvals of responsible local authorities as mentioned in detail in the methods section.

References

1. Aguilar-Calvo P, Sevillano AM, Bapat J, Soldau K, Sandoval DR, Altmeppen HC et al (2020) Shortening heparan sulfate chains prolongs survival and reduces parenchymal plaques in prion disease caused by mobile, ADAM10-cleaved prions. Acta Neuropathol 139:527–546. https://doi.org/10.1007/s00401-019-02085-x
2. Aguzzi A, Baumann F, Bremer J (2008) The prion's elusive reason for being. Annu Rev Neurosci 31:439–477. https://doi.org/10.1146/annurev.neuro.31.060407.125620
3. Aguzzi A, Calella AM (2009) Prions: protein aggregation and infectious diseases. Physiol Rev 89:1105–1152. https://doi.org/10.1152/physrev.00006.2009
4. Altmeppen HC, Prox J, Krasemann S, Puig B, Kruszewski K, Dohler F et al (2015) The sheddase ADAM10 is a potent modulator of prion disease. Elife. https://doi.org/10.7554/eLife.04260

5. Altmeppen HC, Prox J, Puig B, Kluth MA, Bernreuther C, Thurm D et al (2011) Lack of a-disintegrin-and-metalloproteinase ADAM10 leads to intracellular accumulation and loss of shedding of the cellular prion protein in vivo. Mol Neurodegener 6:36. https://doi.org/10.1186/1750-1326-6-36
6. Altmeppen HC, Puig B, Dohler F, Thurm DK, Falker C, Krasemann S et al (2012) Proteolytic processing of the prion protein in health and disease. Am J Neurodegener Dis 1:15–31
7. Amin L, Nguyen XT, Rolle IG, D'Este E, Giachin G, Tran TH et al (2016) Characterization of prion protein function by focal neurite stimulation. J Cell Sci 129:3878–3891. https://doi.org/10.1242/jcs.183137
8. Ballmer BA, Moos R, Liberali P, Pelkmans L, Hornemann S, Aguzzi A (2017) Modifiers of prion protein biogenesis and recycling identified by a highly parallel endocytosis kinetics assay. J Biol Chem 292:8356–8368. https://doi.org/10.1074/jbc.M116.773283
9. Beland M, Roucou X (2012) The prion protein unstructured N-terminal region is a broad-spectrum molecular sensor with diverse and contrasting potential functions. J Neurochem 120:853–868. https://doi.org/10.1111/j.1471-4159.2011.07613.x
10. Benilova I, Reilly M, Terry C, Wenborn A, Schmidt C, Marinho AT et al (2020) Highly infectious prions are not directly neurotoxic. Proc Natl Acad Sci USA 117:23815–23822. https://doi.org/10.1073/pnas.2007406117
11. Bessen RA, Shearin H, Martinka S, Boharski R, Lowe D, Wilham JM et al (2010) Prion shedding from olfactory neurons into nasal secretions. PLoS Pathog 6:e1000837. https://doi.org/10.1371/journal.ppat.1000837
12. Bieschke J, Weber P, Sarafoff N, Beekes M, Giese A, Kretzschmar H (2004) Autocatalytic self-propagation of misfolded prion protein. Proc Natl Acad Sci U S A 101:12207–12211. https://doi.org/10.1073/pnas.0404650101
13. Boon BDC, Bulk M, Jonker AJ, Morrema THJ, van den Berg E, Popovic M et al (2020) The coarse-grained plaque: a divergent Abeta plaque-type in early-onset Alzheimer's disease. Acta Neuropathol 140:811–830. https://doi.org/10.1007/s00401-020-02198-8
14. Borchelt DR, Rogers M, Stahl N, Telling G, Prusiner SB (1993) Release of the cellular prion protein from cultured cells after loss of its glycoinositol phospholipid anchor. Glycobiology 3:319–329
15. Borchelt DR, Scott M, Taraboulos A, Stahl N, Prusiner SB (1990) Scrapie and cellular prion proteins differ in their kinetics of synthesis and topology in cultured cells. J Cell Biol 110:743–752
16. Brenna S, Altmeppen HC, Mohammadi B, Rissiek B, Schlink F, Ludewig P et al (2020) Characterization of brain-derived extracellular vesicles reveals changes in cellular origin after stroke and enrichment of the prion protein with a potential role in cellular uptake. J Extracell Vesicles 9:1809065. https://doi.org/10.1080/20013078.2020.1809065
17. Brummer T, Muller SA, Pan-Montojo F, Yoshida F, Fellgiebel A, Tomita T et al (2019) NrCAM is a marker for substrate-selective activation of ADAM10 in Alzheimer's disease. EMBO Mol Med. https://doi.org/10.15252/emmm.201809695
18. Calella AM, Farinelli M, Nuvolone M, Mirante O, Moos R, Falsig J et al (2010) Prion protein and Abeta-related synaptic toxicity impairment. EMBO Mol Med 2:306–314. https://doi.org/10.1002/emmm.201000082
19. Castle AR, Kang SG, Eskandari-Sedighi G, Wohlgemuth S, Nguyen MA, Drucker DJ et al (2023) Beta-endoproteolysis of the cellular prion protein by dipeptidyl peptidase-4 and fibroblast activation protein. Proc Natl Acad Sci USA 120:e2209815120. https://doi.org/10.1073/pnas.2209815120
20. Chesebro B, Trifilo M, Race R, Meade-White K, Teng C, LaCasse R et al (2005) Anchorless prion protein results in infectious amyloid disease without clinical scrapie. Science 308:1435–1439. https://doi.org/10.1126/science.1110837
21. Collinge J (2001) Prion diseases of humans and animals: their causes and molecular basis. Annu Rev Neurosci 24:519–550
22. Corbett GT, Wang Z, Hong W, Colom-Cadena M, Rose J, Liao M et al (2020) PrP is a central player in toxicity mediated by soluble aggregates of neurodegeneration-causing proteins. Acta Neuropathol 139:503–526. https://doi.org/10.1007/s00401-019-02114-9
23. Curin Serbec V, Bresjanac M, Popovic M, Pretnar Hartman K, Galvani V, Rupreht R et al (2004) Monoclonal antibody against a peptide of human prion protein discriminates between Creutzfeldt–Jacob's disease-affected and normal brain tissue. J Biol Chem 279:3694–3698. https://doi.org/10.1074/jbc.M310868200
24. Dexter E, Kong Q (2021) Neuroprotective effect and potential of cellular prion protein and its cleavage products for treatment of neurodegenerative disorders part II: strategies for therapeutics development. Expert Rev Neurother 21:983–991. https://doi.org/10.1080/14737175.2021.1965882
25. Dohler F, Sepulveda-Falla D, Krasemann S, Altmeppen H, Schluter H, Hildebrand D et al (2014) High molecular mass assemblies of amyloid-beta oligomers bind prion protein in patients with Alzheimer's disease. Brain 137:873–886. https://doi.org/10.1093/brain/awt375
26. Dorey A, Tholance Y, Vighetto A, Perret-Liaudet A, Lachman I, Krolak-Salmon P et al (2015) Association of cerebrospinal fluid prion protein levels and the distinction between Alzheimer disease and Creutzfeldt–Jakob disease. JAMA Neurol 72:267–275. https://doi.org/10.1001/jamaneurol.2014.4068
27. Dvorakova E, Vranac T, Janouskova O, Cernilec M, Koren S, Lukan A et al (2013) Detection of the GPI-anchorless prion protein fragment PrP226* in human brain. BMC Neurol 13:126. https://doi.org/10.1186/1471-2377-13-126
28. Endres K, Mitteregger G, Kojro E, Kretzschmar H, Fahrenholz F (2009) Influence of ADAM10 on prion protein processing and scrapie infectiosity in vivo. Neurobiol Dis 36:233–241. https://doi.org/10.1016/j.nbd.2009.07.015
29. Falker C, Hartmann A, Guett I, Dohler F, Altmeppen H, Betzel C et al (2016) Exosomal cellular prion protein drives fibrillization of amyloid beta and counteracts amyloid beta-mediated neurotoxicity. J Neurochem 137:88–100. https://doi.org/10.1111/jnc.13514
30. Ferreira DG, Temido-Ferreira M, Miranda HV, Batalha VL, Coelho JE, Szego EM et al (2017) alpha-synuclein interacts with PrPC to induce cognitive impairment through mGluR5 and NMDAR2B. Nat Neurosci 20:1569–1579. https://doi.org/10.1038/nn.4648
31. Ferrer I, Blanco R, Carmona M, Puig B, Ribera R, Rey MJ et al (2001) Prion protein expression in senile plaques in Alzheimer's disease. Acta Neuropathol 101:49–56
32. Fischer M, Rülicke T, Raeber A, Sailer A, Moser M, Oesch B et al (1996) Prion protein (PrP) with amino-proximal deletions restoring susceptibility of PrP knockout mice to scrapie. EMBO J 15:1255–1264
33. Fluharty BR, Biasini E, Stravalaci M, Sclip A, Diomede L, Balducci C et al (2013) An N-terminal fragment of the prion protein binds to amyloid-beta oligomers and inhibits their neurotoxicity in vivo. J Biol Chem 288:7857–7866. https://doi.org/10.1074/jbc.M112.423954
34. Ghetti B, Piccardo P, Frangione B, Bugiani O, Giaccone G, Young K et al (1996) Prion protein amyloidosis. Brain Pathol 6:127–145
35. Ghetti B, Piccardo P, Spillantini MG, Ichimiya Y, Porro M, Perini F et al (1996) Vascular variant of prion protein cerebral amyloidosis with tau-positive neurofibrillary tangles: the phenotype of

the stop codon 145 mutation in PRNP. Proc Natl Acad Sci USA 93:744–748
36. Gomes LA, Hipp SA, Rijal Upadhaya A, Balakrishnan K, Ospitalieri S, Koper MJ et al (2019) Abeta-induced acceleration of Alzheimer-related tau-pathology spreading and its association with prion protein. Acta Neuropathol. https://doi.org/10.1007/s00401-019-02053-5
37. Guner G, Assfalg M, Zhao K, Dreyer T, Lahiri S, Lo Y et al (2022) Proteolytically generated soluble Tweak Receptor Fn14 is a blood biomarker for gamma-secretase activity. EMBO Mol Med 14:e16084. https://doi.org/10.15252/emmm.202216084
38. Haass C, Selkoe DJ (2007) Soluble protein oligomers in neurodegeneration: lessons from the Alzheimer's amyloid beta-peptide. Nat Rev Mol Cell Biol 8:101–112. https://doi.org/10.1038/nrm2101
39. Haddon DJ, Hughes MR, Antignano F, Westaway D, Cashman NR, McNagny KM (2009) Prion protein expression and release by mast cells after activation. J Infect Dis 200:827–831. https://doi.org/10.1086/605022
40. Harris DA, Huber MT, van Dijken P, Shyng SL, Chait BT, Wang R (1993) Processing of a cellular prion protein: identification of N- and C-terminal cleavage sites. Biochemistry 32:1009–1016
41. Hartmann D, de Strooper B, Serneels L, Craessaerts K, Herreman A, Annaert W et al (2002) The disintegrin/metalloprotease ADAM 10 is essential for Notch signalling but not for alpha-secretase activity in fibroblasts. Hum Mol Genet 11:2615–2624
42. Heiseke A, Schobel S, Lichtenthaler SF, Vorberg I, Groschup MH, Kretzschmar H et al (2008) The novel sorting nexin SNX33 interferes with cellular PrP formation by modulation of PrP shedding. Traffic 9:1116–1129. https://doi.org/10.1111/j.1600-0854.2008.00750.x
43. Hong W, Wang Z, Liu W, O'Malley TT, Jin M, Willem M et al (2018) Diffusible, highly bioactive oligomers represent a critical minority of soluble Abeta in Alzheimer's disease brain. Acta Neuropathol 136:19–40. https://doi.org/10.1007/s00401-018-1846-7
44. Horiuchi M, Priola SA, Chabry J, Caughey B (2000) Interactions between heterologous forms of prion protein: binding, inhibition of conversion, and species barriers [In Process Citation]. Proc Natl Acad Sci USA 97:5836–5841
45. Hundhausen C, Misztela D, Berkhout TA, Broadway N, Saftig P, Reiss K et al (2003) The disintegrin-like metalloproteinase ADAM10 is involved in constitutive cleavage of CX3CL1 (fractalkine) and regulates CX3CL1-mediated cell-cell adhesion. Blood 102:1186–1195. https://doi.org/10.1182/blood-2002-12-3775
46. Jansen C, Parchi P, Capellari S, Vermeij AJ, Corrado P, Baas F et al (2010) Prion protein amyloidosis with divergent phenotype associated with two novel nonsense mutations in PRNP. Acta Neuropathol 119:189–197. https://doi.org/10.1007/s00401-009-0609-x
47. Jarosz-Griffiths HH, Corbett NJ, Rowland HA, Fisher K, Jones AC, Baron J et al (2019) Proteolytic shedding of the prion protein via activation of metallopeptidase ADAM10 reduces cellular binding and toxicity of amyloid-beta oligomers. J Biol Chem 294:7085–7097. https://doi.org/10.1074/jbc.RA118.005364
48. Jimenez-Huete A, Lievens PM, Vidal R, Piccardo P, Ghetti B, Tagliavini F et al (1998) Endogenous proteolytic cleavage of normal and disease-associated isoforms of the human prion protein in neural and non-neural tissues. Am J Pathol 153:1561–1572. https://doi.org/10.1016/S0002-9440(10)65744-6
49. Jocher G, Grass V, Tschirner SK, Riepler L, Breimann S, Kaya T et al (2022) ADAM10 and ADAM17 promote SARS-CoV-2 cell entry and spike protein-mediated lung cell fusion. EMBO Rep 23:e54305. https://doi.org/10.15252/embr.202154305
50. Jorissen E, Prox J, Bernreuther C, Weber S, Schwanbeck R, Serneels L et al (2010) The disintegrin/metalloproteinase ADAM10 is essential for the establishment of the brain cortex. J Neurosci 30:4833–4844. https://doi.org/10.1523/JNEUROSCI.5221-09.2010
51. Kobayashi A, Hirata T, Nishikaze T, Ninomiya A, Maki Y, Takada Y et al (2020) alpha2,3 linkage of sialic acid to a GPI anchor and an unpredicted GPI attachment site in human prion protein. J Biol Chem 295:7789–7798. https://doi.org/10.1074/jbc.RA120.013444
52. Kohutek ZA, diPierro CG, Redpath GT, Hussaini IM (2009) ADAM-10-mediated N-cadherin cleavage is protein kinase C-alpha dependent and promotes glioblastoma cell migration. J Neurosci 29:4605–4615. https://doi.org/10.1523/JNEUROSCI.5126-08.2009
53. Kopycka K, Maddison BC, Gough KC (2023) Recombinant ovine prion protein can be mutated at position 136 to improve its efficacy as an inhibitor of prion propagation. Sci Rep 13:3452. https://doi.org/10.1038/s41598-023-30202-0
54. Kosmac M, Koren S, Giachin G, Stoilova T, Gennaro R, Legname G et al (2011) Epitope mapping of a PrP(Sc)-specific monoclonal antibody: identification of a novel C-terminally truncated prion fragment. Mol Immunol 48:746–750. https://doi.org/10.1016/j.molimm.2010.11.012
55. Kovac V, Curin Serbec V (2022) Prion protein: the molecule of many forms and faces. Int J Mol Sci. https://doi.org/10.3390/ijms23031232
56. Kovac V, Hafner-Bratkovic I, Curin Serbec V (2016) Anchorless forms of prion protein—impact of truncation on structure destabilization and prion protein conversion. Biochem Biophys Res Commun 481:1–6. https://doi.org/10.1016/j.bbrc.2016.11.036
57. Kovac V, Serbec VC (2018) Prion proteins without the glycophosphatidylinositol anchor: potential biomarkers in neurodegenerative diseases. Biomark Insights. https://doi.org/10.1177/1177271918756648
58. Kovac V, Zupancic B, Ilc G, Plavec J, Curin Serbec V (2017) Truncated prion protein PrP226*—a structural view on its role in amyloid disease. Biochem Biophys Res Commun 484:45–50. https://doi.org/10.1016/j.bbrc.2017.01.078
59. Kuffer A, Lakkaraju AK, Mogha A, Petersen SC, Airich K, Doucerain C et al (2016) The prion protein is an agonistic ligand of the G protein-coupled receptor Adgrg6. Nature 536:464–468. https://doi.org/10.1038/nature19312
60. Kuhn PH, Wang H, Dislich B, Colombo A, Zeitschel U, Ellwart JW et al (2010) ADAM10 is the physiologically relevant, constitutive alpha-secretase of the amyloid precursor protein in primary neurons. EMBO J 29:3020–3032. https://doi.org/10.1038/emboj.2010.167
61. Laffont-Proust I, Faucheux BA, Hassig R, Sazdovitch V, Simon S, Grassi J et al (2005) The N-terminal cleavage of cellular prion protein in the human brain. FEBS Lett 579:6333–6337. https://doi.org/10.1016/j.febslet.2005.10.013
62. Lambert MP, Barlow AK, Chromy BA, Edwards C, Freed R, Liosatos M et al (1998) Diffusible, nonfibrillar ligands derived from Abeta1-42 are potent central nervous system neurotoxins. Proc Natl Acad Sci USA 95:6448–6453
63. Lancaster MA, Knoblich JA (2014) Generation of cerebral organoids from human pluripotent stem cells. Nat Protoc 9:2329–2340. https://doi.org/10.1038/nprot.2014.158
64. Lauren J, Gimbel DA, Nygaard HB, Gilbert JW, Strittmatter SM (2009) Cellular prion protein mediates impairment of synaptic plasticity by amyloid-beta oligomers. Nature 457:1128–1132. https://doi.org/10.1038/nature07761

65. Lee YK, Uchida H, Smith H, Ito A, Sanchez T (2019) The isolation and molecular characterization of cerebral microvessels. Nat Protoc 14:3059–3081. https://doi.org/10.1038/s41596-019-0212-0
66. Lewis V, Johanssen VA, Crouch PJ, Klug GM, Hooper NM, Collins SJ (2016) Prion protein "gamma-cleavage": characterizing a novel endoproteolytic processing event. Cell Mol Life Sci 73:667–683. https://doi.org/10.1007/s00018-015-2022-z
67. Lichtenthaler SF, Lemberg MK, Fluhrer R (2018) Proteolytic ectodomain shedding of membrane proteins in mammals-hardware, concepts, and recent developments. EMBO J. https://doi.org/10.15252/embj.201899456
68. Lichtenthaler SF, Tschirner SK, Steiner H (2022) Secretases in Alzheimer's disease: novel insights into proteolysis of APP and TREM2. Curr Opin Neurobiol 72:101–110. https://doi.org/10.1016/j.conb.2021.09.003
69. Linden R, Cordeiro Y, Lima LM (2012) Allosteric function and dysfunction of the prion protein. Cell Mol Life Sci 69:1105–1124. https://doi.org/10.1007/s00018-011-0847-7
70. Linsenmeier L, Altmeppen HC, Wetzel S, Mohammadi B, Saftig P, Glatzel M (2017) Diverse functions of the prion protein—does proteolytic processing hold the key? Biochim Biophys Acta 1864:2128–2137. https://doi.org/10.1016/j.bbamcr.2017.06.022
71. Linsenmeier L, Mohammadi B, Shafiq M, Frontzek K, Bar J, Shrivastava AN et al (2021) Ligands binding to the prion protein induce its proteolytic release with therapeutic potential in neurodegenerative proteinopathies. Sci Adv 7:eabj1826. https://doi.org/10.1126/sciadv.abj1826
72. Linsenmeier L, Mohammadi B, Wetzel S, Puig B, Jackson WS, Hartmann A et al (2018) Structural and mechanistic aspects influencing the ADAM10-mediated shedding of the prion protein. Mol Neurodegener 13:18. https://doi.org/10.1186/s13024-018-0248-6
73. Lipper CH, Egan ED, Gabriel KH, Blacklow SC (2023) Structural basis for membrane-proximal proteolysis of substrates by ADAM10. Cell. https://doi.org/10.1016/j.cell.2023.06.026
74. London N, Raveh B, Cohen E, Fathi G, Schueler-Furman O (2011) Rosetta FlexPepDock web server–high resolution modeling of peptide-protein interactions. Nucleic Acids Res 39:W249-253. https://doi.org/10.1093/nar/gkr431
75. Lukan A, Cernilec M, Vranac T, Popovic M, Curin Serbec V (2014) Regional distribution of anchorless prion protein, PrP226*, in the human brain. Prion 8:203–209. https://doi.org/10.4161/pri.28388
76. MacGregor I, Hope J, Barnard G, Kirby L, Drummond O, Pepper D et al (1999) Application of a time-resolved fluoroimmunoassay for the analysis of normal prion protein in human blood and its components. Vox Sang 77:88–96
77. Manka SW, Wenborn A, Collinge J, Wadsworth JDF (2023) Prion strains viewed through the lens of cryo-EM. Cell Tissue Res 392:167–178. https://doi.org/10.1007/s00441-022-03676-z
78. Mantuano E, Azmoon P, Banki MA, Lam MS, Sigurdson CJ, Gonias SL (2020) A soluble derivative of PrP(C) activates cell-signaling and regulates cell physiology through LRP1 and the NMDA receptor. J Biol Chem 295:14178–14188. https://doi.org/10.1074/jbc.RA120.013779
79. Mantuano E, Azmoon P, Banki MA, Sigurdson CJ, Campana WM, Gonias SL (2022) A Soluble PrP(C) derivative and membrane-anchored PrP(C) in extracellular vesicles attenuate innate immunity by engaging the NMDA-R/LRP1 receptor complex. J Immunol 208:85–96. https://doi.org/10.4049/jimmunol.2100412
80. Mantuano E, Zampieri C, Azmoon P, Gunner CB, Heye KR, Gonias SL (2023) An LRP1-binding motif in cellular prion protein replicates cell-signaling activities of the full-length protein. JCI Insight. https://doi.org/10.1172/jci.insight.170121
81. Martellucci S, Santacroce C, Santilli F, Piccoli L, Delle Monache S, Angelucci A et al (2019) Cellular and molecular mechanisms mediated by recPrP(C) involved in the neuronal differentiation process of mesenchymal stem cells. Int J Mol Sci. https://doi.org/10.3390/ijms20020345
82. Mathiason CK, Powers JG, Dahmes SJ, Osborn DA, Miller KV, Warren RJ et al (2006) Infectious prions in the saliva and blood of deer with chronic wasting disease. Science 314:133–136. https://doi.org/10.1126/science.1132661
83. McDonald AJ, Dibble JP, Evans EG, Millhauser GL (2014) A new paradigm for enzymatic control of alpha-cleavage and beta-cleavage of the prion protein. J Biol Chem 289:803–813. https://doi.org/10.1074/jbc.M113.502351
84. Mead S, Gandhi S, Beck J, Caine D, Gallujipali D, Carswell C et al (2013) A novel prion disease associated with diarrhea and autonomic neuropathy. N Engl J Med 369:1904–1914
85. Mead S, Khalili-Shirazi A, Potter C, Mok T, Nihat A, Hyare H et al (2022) Prion protein monoclonal antibody (PRN100) therapy for Creutzfeldt–Jakob disease: evaluation of a first-in-human treatment programme. Lancet Neurol 21:342–354. https://doi.org/10.1016/S1474-4422(22)00082-5
86. Megra BW, Eugenin EA, Berman JW (2017) The role of shed PrPc in the neuropathogenesis of HIV infection. J Immunol 199:224–232. https://doi.org/10.4049/jimmunol.1601041
87. Mehrabian M, Wang X, Eid S, Yan BQ, Grinberg M, Siegner M et al (2022) Cardiac glycoside-mediated turnover of Na, K-ATPases as a rational approach to reducing cell surface levels of the cellular prion protein. PLoS ONE 17:e0270915. https://doi.org/10.1371/journal.pone.0270915
88. Meier P, Genoud N, Prinz M, Maissen M, Rulicke T, Zurbriggen A et al (2003) Soluble dimeric prion protein binds PrP(Sc) in vivo and antagonizes prion disease. Cell 113:49–60
89. Meyne F, Gloeckner SF, Ciesielczyk B, Heinemann U, Krasnianski A, Meissner B et al (2009) Total prion protein levels in the cerebrospinal fluid are reduced in patients with various neurological disorders. J Alzheimers Dis 17:863–873. https://doi.org/10.3233/JAD-2009-1110
90. Minikel EV, Kuhn E, Cocco AR, Vallabh SM, Hartigan CR, Reidenbach AG et al (2019) Domain-specific quantification of prion protein in cerebrospinal fluid by targeted mass spectrometry. Mol Cell Proteom 18:2388–2400. https://doi.org/10.1074/mcp.RA119.001702
91. Minikel EV, Zhao HT, Le J, O'Moore J, Pitstick R, Graffam S et al (2020) Prion protein lowering is a disease-modifying therapy across prion disease stages, strains and endpoints. Nucleic Acids Res 48:10615–10631. https://doi.org/10.1093/nar/gkaa616
92. Mohammadi B, Linsenmeier L, Shafiq M, Puig B, Galliciotti G, Giudici C et al (2020) Transgenic overexpression of the disordered prion protein N1 fragment in mice does not protect against neurodegenerative diseases due to impaired ER translocation. Mol Neurobiol 57:2812–2829. https://doi.org/10.1007/s12035-020-01917-2
93. Mohammadi B, Song F, Matamoros-Angles A, Shafiq M, Damme M, Puig B et al (2022) Anchorless risk or released benefit? An updated view on the ADAM10-mediated shedding of the prion protein. Cell Tissue Res. https://doi.org/10.1007/s00441-022-03582-4
94. Mortberg MA, Gentile JE, Nadaf NM, Vanderburg C, Simmons S, Dubinsky D et al (2023) A single-cell map of antisense oligonucleotide activity in the brain. Nucleic Acids Res. https://doi.org/10.1093/nar/gkad371
95. Nieznanski K, Choi JK, Chen S, Surewicz K, Surewicz WK (2012) Soluble prion protein inhibits amyloid-beta (abeta) fibrillization and toxicity. J Biol Chem 287:33104–33108. https://doi.org/10.1074/jbc.C112.400614

96. Ondrejcak T, Klyubin I, Corbett GT, Fraser G, Hong W, Mably AJ et al (2018) Cellular prion protein mediates the disruption of hippocampal synaptic plasticity by soluble tau in vivo. J Neurosci 38:10595–10606. https://doi.org/10.1523/JNEUROSCI.1700-18.2018
97. Paquet C, Privat N, Kaci R, Polivka M, Dupont O, Haik S et al (2008) Cerebral amyloid angiopathy with co-localization of prion protein and beta-amyloid in an 85-year-old patient with sporadic Creutzfeldt–Jakob disease. Acta Neuropathol 116:567–573. https://doi.org/10.1007/s00401-008-0394-y
98. Parizek P, Roeckl C, Weber J, Flechsig E, Aguzzi A, Raeber AJ (2001) Similar turnover and shedding of the cellular prion protein in primary lymphoid and neuronal cells. J Biol Chem 276:44627–44632. https://doi.org/10.1074/jbc.M107458200
99. Perini F, Frangione B, Prelli F (1996) Prion protein released by platelets. Lancet 347:1635–1636
100. Piccardo P, Ghetti B, Dickson DW, Vinters HV, Giaccone G, Bugiani O et al (1995) Gerstmann–Straussler–Scheinker disease (PRNP P102L): amyloid deposits are best recognized by antibodies directed to epitopes in PrP region 90–165. J Neuropathol Exp Neurol 54:790–801
101. Provenzano L, Ryan Y, Hilton DA, Lyons-Rimmer J, Dave F, Maze EA et al (2017) Cellular prion protein (PrPC) in the development of Merlin-deficient tumours. Oncogene. https://doi.org/10.1038/onc.2017.200
102. Prox J, Bernreuther C, Altmeppen H, Grendel J, Glatzel M, D'Hooge R et al (2013) Postnatal disruption of the disintegrin/metalloproteinase ADAM10 in brain causes epileptic seizures, learning deficits, altered spine morphology, and defective synaptic functions. J Neurosci 33(12915–12928):12928a. https://doi.org/10.1523/JNEUROSCI.5910-12.2013
103. Prusiner SB (1982) Novel proteinaceous infectious particles cause scrapie. Science 216:136–144
104. Raymond GJ, Zhao HT, Race B, Raymond LD, Williams K, Swayze EE et al (2019) Antisense oligonucleotides extend survival of prion-infected mice. JCI Insight. https://doi.org/10.1172/jci.insight.131175
105. Resenberger UK, Harmeier A, Woerner AC, Goodman JL, Muller V, Krishnan R et al (2011) The cellular prion protein mediates neurotoxic signalling of beta-sheet-rich conformers independent of prion replication. EMBO J 30:2057–2070. https://doi.org/10.1038/emboj.2011.86
106. Roberts TK, Eugenin EA, Morgello S, Clements JE, Zink MC, Berman JW (2010) PrPC, the cellular isoform of the human prion protein, is a novel biomarker of HIV-associated neurocognitive impairment and mediates neuroinflammation. Am J Pathol 177:1848–1860. https://doi.org/10.2353/ajpath.2010.091006
107. Rosenbaum D, Saftig P (2023) New insights into the function and pathophysiology of the ectodomain sheddase A disintegrin and metalloproteinase 10 (ADAM10). FEBS J. https://doi.org/10.1111/febs.16870
108. Saftig P, Lichtenthaler SF (2015) The alpha secretase ADAM10: a metalloprotease with multiple functions in the brain. Prog Neurobiol. https://doi.org/10.1016/j.pneurobio.2015.10.003
109. Sandberg MK, Al-Doujaily H, Sharps B, Clarke AR, Collinge J (2011) Prion propagation and toxicity in vivo occur in two distinct mechanistic phases. Nature 470:540–542. https://doi.org/10.1038/nature09768
110. Scharfenberg F, Helbig A, Sammel M, Benzel J, Schlomann U, Peters F et al (2020) Degradome of soluble ADAM10 and ADAM17 metalloproteases. Cell Mol Life Sci 77:331–350. https://doi.org/10.1007/s00018-019-03184-4
111. Schlondorff J, Becherer JD, Blobel CP (2000) Intracellular maturation and localization of the tumour necrosis factor alpha convertase (TACE). Biochem J 347(Pt 1):131–138
112. Schwarze-Eicker K, Keyvani K, Gortz N, Westaway D, Sachser N, Paulus W (2005) Prion protein (PrPc) promotes beta-amyloid plaque formation. Neurobiol Aging 26:1177–1182
113. Scott-McKean JJ, Surewicz K, Choi JK, Ruffin VA, Salameh AI, Nieznanski K et al (2016) Soluble prion protein and its N-terminal fragment prevent impairment of synaptic plasticity by Abeta oligomers: Implications for novel therapeutic strategy in Alzheimer's disease. Neurobiol Dis 91:124–131. https://doi.org/10.1016/j.nbd.2016.03.001
114. Seegar TCM, Killingsworth LB, Saha N, Meyer PA, Patra D, Zimmerman B et al (2017) Structural basis for regulated proteolysis by the alpha-secretase ADAM10. Cell 171(1638–1648):e1637. https://doi.org/10.1016/j.cell.2017.11.014
115. Seipold L, Altmeppen H, Koudelka T, Tholey A, Kasparek P, Sedlacek R et al (2018) In vivo regulation of the A disintegrin and metalloproteinase 10 (ADAM10) by the tetraspanin 15. Cell Mol Life Sci. https://doi.org/10.1007/s00018-018-2791-2
116. Sevillano AM, Aguilar-Calvo P, Kurt TD, Lawrence JA, Soldau K, Nam TH et al (2020) Prion protein glycans reduce intracerebral fibril formation and spongiosis in prion disease. J Clin Invest 130:1350–1362. https://doi.org/10.1172/JCI131564
117. Skrlj N, Vranac T, Popovic M, Curin Serbec V, Dolinar M (2011) Specific binding of the pathogenic prion isoform: development and characterization of a humanized single-chain variable antibody fragment. PLoS ONE 6:e15783. https://doi.org/10.1371/journal.pone.0015783
118. Stahl N, Borchelt DR, Prusiner SB (1990) Differential release of cellular and scrapie prion proteins from cellular membranes by phosphatidylinositol-specific phospholipase C. Biochemistry 29:5405–5412
119. Stohr J, Watts JC, Legname G, Oehler A, Lemus A, Nguyen HO et al (2011) Spontaneous generation of anchorless prions in transgenic mice. Proc Natl Acad Sci USA 108:21223–21228. https://doi.org/10.1073/pnas.1117827108
120. Tagliavini F, Prelli F, Porro M, Salmona M, Bugiani O, Frangione B (1992) A soluble form of prion protein in human cerebrospinal fluid: implications for prion-related encephalopathies. Biochem Biophys Res Commun 184:1398–1404
121. Takahashi RH, Yokotsuka M, Tobiume M, Sato Y, Hasegawa H, Nagao T et al (2021) Accumulation of cellular prion protein within beta-amyloid oligomer plaques in aged human brains. Brain Pathol. https://doi.org/10.1111/bpa.12941
122. Taylor DR, Parkin ET, Cocklin SL, Ault JR, Ashcroft AE, Turner AJ et al (2009) Role of ADAMs in the ectodomain shedding and conformational conversion of the prion protein. J Biol Chem 284:22590–22600. https://doi.org/10.1074/jbc.M109.032599
123. Telling GC, Parchi P, DeArmond SJ, Cortelli P, Montagna P, Gabizon R et al (1996) Evidence for the conformation of the pathologic isoform of the prion protein enciphering and propagating prion diversity. Science 274:2079–2082
124. Tennant JM, Li M, Henderson DM, Tyer ML, Denkers ND, Haley NJ et al (2020) Shedding and stability of CWD prion seeding activity in cervid feces. PLoS ONE 15:e0227094. https://doi.org/10.1371/journal.pone.0227094
125. Thevenet P, Shen Y, Maupetit J, Guyon F, Derreumaux P, Tuffery P (2012) PEP-FOLD: an updated de novo structure prediction server for both linear and disulfide bonded cyclic peptides. Nucleic Acids Res 40:W288-293. https://doi.org/10.1093/nar/gks419
126. Thune K, Schmitz M, Villar-Pique A, Altmeppen HC, Schlomm M, Zafar S et al (2019) The cellular prion protein and its derived fragments in human prion diseases and their role as potential biomarkers. Expert Rev Mol Diagn 19:1007–1018. https://doi.org/10.1080/14737159.2019.1667231

127. Tucher J, Linke D, Koudelka T, Cassidy L, Tredup C, Wichert R et al (2014) LC-MS based cleavage site profiling of the proteases ADAM10 and ADAM17 using proteome-derived peptide libraries. J Proteome Res 13:2205–2214. https://doi.org/10.1021/pr401135u
128. Ulrih NP, Skrt M, Veranic P, Galvani V, Vranac T, Curin Serbec V (2006) Oligomeric forms of peptide fragment PrP(214–226) in solution are preferentially recognized by PrP(Sc)-specific antibody. Biochem Biophys Res Commun 344:1320–1326. https://doi.org/10.1016/j.bbrc.2006.04.046
129. Vallabh SM, Nobuhara CK, Llorens F, Zerr I, Parchi P, Capellari S et al (2019) Prion protein quantification in human cerebrospinal fluid as a tool for prion disease drug development. Proc Natl Acad Sci USA 116:7793–7798. https://doi.org/10.1073/pnas.1901947116
130. Vanni I, Iacobone F, D'Agostino C, Giovannelli M, Pirisinu L, Altmeppen HC et al (2022) An optimized Western blot assay provides a comprehensive assessment of the physiological endoproteolytic processing of the prion protein. J Biol Chem 299:102823. https://doi.org/10.1016/j.jbc.2022.102823
131. Viola KL, Klein WL (2015) Amyloid beta oligomers in Alzheimer's disease pathogenesis, treatment, and diagnosis. Acta Neuropathol 129:183–206. https://doi.org/10.1007/s00401-015-1386-3
132. Vranac T, Hartman KP, Popovic M, Venturini A, Zerovnik E, Curin Serbec V (2006) A single prion protein peptide can elicit a panel of isoform specific monoclonal antibodies. Peptides 27:2695–2705. https://doi.org/10.1016/j.peptides.2006.05.026
133. Walsh DM, Klyubin I, Fadeeva JV, Cullen WK, Anwyl R, Wolfe MS et al (2002) Naturally secreted oligomers of amyloid beta protein potently inhibit hippocampal long-term potentiation in vivo. Nature 416:535–539. https://doi.org/10.1038/416535a
134. Wetzel S, Seipold L, Saftig P (2017) The metalloproteinase ADAM10: a useful therapeutic target? Biochim Biophys Acta. https://doi.org/10.1016/j.bbamcr.2017.06.005
135. Wiegmans AP, Saunus JM, Ham S, Lobb R, Kutasovic JR, Dalley AJ et al (2019) Secreted cellular prion protein binds doxorubicin and correlates with anthracycline resistance in breast cancer. JCI Insight. https://doi.org/10.1172/jci.insight.124092
136. Yuan J, Zhan YA, Abskharon R, Xiao X, Martinez MC, Zhou X et al (2013) Recombinant human prion protein inhibits prion propagation in vitro. Sci Rep 3:2911. https://doi.org/10.1038/srep02911

Authors and Affiliations

Feizhi Song[1] · Valerija Kovac[2] · Behnam Mohammadi[1] · Jessica L. Littau[1] · Franka Scharfenberg[3] · Andreu Matamoros Angles[1] · Ilaria Vanni[4] · Mohsin Shafiq[1] · Leonor Orge[5,6] · Giovanna Galliciotti[1] · Salma Djakkani[1] · Luise Linsenmeier[1] · Maja Černilec[2] · Katrina Hartman[2] · Sebastian Jung[7] · Jörg Tatzelt[7,8] · Julia E. Neumann[1,9] · Markus Damme[3] · Sarah K. Tschirner[10,11] · Stefan F. Lichtenthaler[10,11,12] · Franz L. Ricklefs[13] · Thomas Sauvigny[13] · Matthias Schmitz[14] · Inga Zerr[14] · Berta Puig[15] · Eva Tolosa[16] · Isidro Ferrer[17] · Tim Magnus[15] · Marjan S. Rupnik[18] · Diego Sepulveda-Falla[1] · Jakob Matschke[1] · Lojze M. Šmid[19] · Mara Bresjanac[19] · Olivier Andreoletti[20] · Susanne Krasemann[1] · Simote T. Foliaki[21] · Romolo Nonno[4] · Christoph Becker-Pauly[3] · Cecile Monzo[22] · Carole Crozet[22] · Cathryn L. Haigh[21] · Markus Glatzel[1] · Vladka Curin Serbec[2] · Hermann C. Altmeppen[1]

✉ Vladka Curin Serbec
vladka.curin@ztm.si

✉ Hermann C. Altmeppen
h.altmeppen@uke.de

1 Institute of Neuropathology, University Medical Center Hamburg-Eppendorf (UKE), Hamburg, Germany

2 Centre for Immunology and Development, Blood Transfusion Centre of Slovenia (BTCS), Ljubljana, Slovenia

3 Institute of Biochemistry, University of Kiel, Kiel, Germany

4 Department of Food Safety and Veterinary Public Health, Istituto Superiore di Sanità, Rome, Italy

5 National Institute for Agricultural and Veterinary Research (INIAV), Oeiras, Portugal

6 Animal and Veterinary Research Centre (CECAV), University of Trás-os-Montes and Alto Douro (UTAD), Vila Real, Portugal

7 Department of Biochemistry of Neurodegenerative Diseases, Institute of Biochemistry and Pathobiochemistry, Ruhr University Bochum, Bochum, Germany

8 Cluster of Excellence RESOLV, Ruhr University Bochum, Bochum, Germany

9 Center for Molecular Neurobiology Hamburg (ZMNH), UKE, Hamburg, Germany

10 German Center for Neurodegenerative Diseases (DZNE), Munich, Germany

11 Neuroproteomics, School of Medicine and Health, Klinikum rechts der Isar, Technical University Munich, 81675 Munich, Germany

12 Munich Cluster for Systems Neurology (SyNergy), Munich, Germany

13 Department of Neurosurgery, University Medical Center Hamburg-Eppendorf (UKE), Hamburg, Germany

14 Department of Neurology, University Medical Center Göttingen, Göttingen, Germany

15 Department of Neurology, Experimental Research in Stroke and Inflammation (ERSI), UKE, Hamburg, Germany

16 Department of Immunology, University Medical Center Hamburg-Eppendorf (UKE), Hamburg, Germany

17 Department of Pathology and Experimental Therapeutics, University of Barcelona, IDIBELL, Hospitalet de Llobregat, Spain

18 Center for Physiology and Pharmacology, Medical University of Vienna, Vienna, Austria

[19] LNPR, Institute of Pathophysiology and Prion Laboratory, Institute of Pathology, Faculty of Medicine, University of Ljubljana, Ljubljana, Slovenia

[20] UMR INRAE ENVT 1225, Interactions Hôtes-Agents Pathogènes, École Nationale Vétérinaire de Toulouse, Toulouse, France

[21] Laboratory of Persistent Viral Diseases, Division of Intramural Research, Rocky Mountain Laboratories, National Institutes of Health, Hamilton, MT, USA

[22] Institute for Regenerative Medicine and Biotherapies (IRMB), Neural Stem Cell, MSC and Neurodegenerative Diseases, INSERM, Montpellier, France